Measurement and Modeling of McKibben Pneumatic Artificial Muscles

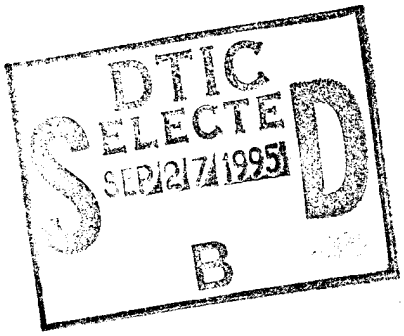

Ching-Ping Chou

Blake Hannaford

Department of Electrical Engineering

FT-10

University of Washington

Seattle, Washington 98195

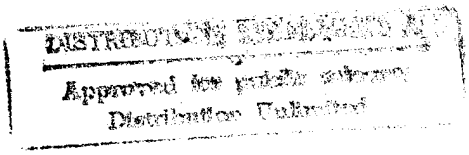

Abstract: This paper reports mechanical testing and modeling results for the McKibben artificial muscle pneumatic actuator. This device, first developed in the 1950's, contains an expanding tube surrounded by braided cords. We report static and dynamic length-tension testing results and derive a linearized model of these properties for three different models. The results are briefly compared with human muscle properties to evaluate the suitability of McKibben actuators for human muscle emulation in biologically based robot arms.

Introduction

The McKibben pneumatic artificial muscle was developed in artificial limb research in the 1950s and 1960s (Schulte 1961, Gavrilovic and Maric 1969). They have recently been commercialized by the Bridgestone Rubber Company of Japan for robotic applications, and re-engineered by Prof. Jack Winters for construction of biomechanically realistic skeletal models. McKibben muscles consist of an internal bladder surrounded by a braided mesh shell (with flexible yet non-extensible threads) that is attached at either end to fittings or to some tendon-like structure (Fig. 1a). When the internal bladder is pressurized, the high pressure gas pushes against its inner surface and against the external shell, and tends to increase its volume. Due to the non-extensibility (or very high longitudinal stiffness) of the threads in the braided mesh shell, the actuator shortens according to its volume increase and/or produces tension if it is coupled to a mechanical load. This physical configuration causes McKibben muscles to have variable-stiffness spring-like characteristics, non-linear passive elasticity, physical flexibility, and very light weight compare to other kinds of artificial actuators (Hannaford and Winters 1990).

The relationships between tension, length, velocity, and activation are major characteristics of actuators which vary greatly from type to type. Human skeletal muscle also has its own particular characteristics: for example, the convex shape active tension-length relationship (Gordon et al. 1966), the non-linear passive tension-length relationship, the hyperbolic tension-velocity relationship (Hill 1938). Each of these properties is also a function of activation level (McMahon 1984, Winters 1990, Zahalak 1990). In order to show the similarity (or not) to biological muscles, three types of McKibben muscles, two designed and made by Dr. Winters and one manufactured by Bridgestone, were tested. Also, since the actuator is pneumatically driven, experiments and modeling on simple pneumatic circuits were included.

In this article, all of the experiments, theories, modeling, and simulations are grouped into four major parts: part I, quasi-static and dynamic tension-length relationships, part II, pneumatic circuits, part III, isometric and isotonic experiments, and part IV, energy conversion and efficiency estimation.

In part I, 1) an idealized static physical model of McKibben muscles will be analyzed with a simple theoretical approach, 2) a dynamic testing machine will be described, 3) a series of quasi-static and dynamic experiments will be described, which show a velocity insensitive tension-length hysteresis, 4) a simplified static model will be described based on both experimental data and a theoretical approach, and 5) the quasi-static and dynamic characteristics will be analyzed. In part II, 1) two dynamic experiments will be described with simple pneumatic circuits, and 2) lumped parameter models with linear or nonlinear gas resistance will be described and simulated. In part III, isometric and isotonic experiments related to the pneumatic behavior will be shown. In part IV, energy conversion and efficiency based on gas dynamics and thermodynamics will be estimated.

Finally, the actuators and pneumatic system will be compared to biological muscles. In general, the McKibben artificial muscle is much more similar to biological muscles than other kinds of artificial actuators. However, the pneumatic system, which provides control and power to the actuator, still needs a lot of improvement in order to be implemented into a feasible, independent

system.

Part I Static and dynamic tension-length relationships

McKibben muscle is an actuator which converts pneumatic (or hydraulic) energy into mechanical form by transferring the pressure applied on the inner surface of its bladder into the shortening tension. To find the relationship of the tension, length, and pressure, a theoretical approach and several experiments will be analyzed with simplified modeling.

1) Static physical model of McKibben muscles

In order to find the tension as a function of pressure and actuator length without considering the detailed geometric structure, a theoretical approach based on energy conservation is described as follows.

The input work (W_{in}) is done in the McKibben muscle when gas pushes the inner bladder surface. This is

$$dW_{in} = \int_{S_i} (P - P_o)\, d\mathbf{l_i} \cdot d\mathbf{s_i} = (P - P_o) \int_{S_i} d\mathbf{l_i} \cdot d\mathbf{s_i} = P' dV \tag{1}$$

where P is the absolute internal gas pressure, P_o, the environment pressure (1 atm = 1.0336 bar), P', the relative pressure, S_i, the total inner surface, $d\mathbf{s_i}$, the area vector, $d\mathbf{l_i}$, the inner surface displacement, and dV, the volume change. The output work (W_{out}) is done when the actuator shortens associated with the volume change, which is

$$dW_{out} = -FdL \tag{2}$$

where F is the axial tension, and dL, the axial displacement. From the view of energy conservation, the input work should equal the output work if a system is lossless and without energy storage. Assume the actuator is in this ideal condition. We can then use the "virtual work" argument:

$$dW_{out} = dW_{in}, \tag{3}$$

thus, from equ. 1 and equ. 2,

$$-FdL = P'dV, \tag{4a}$$

$$F = -P'\frac{dV}{dL}. \tag{4b}$$

To estimate dV/dL, the middle portion of the actuator is modeled as a perfect cylinder (Fig. 1b), where L is the length of the cylinder, θ, the angle between a braided thread and the cylinder long axis, D, the diameter of the cylinder, n, number of turns of a thread, and b, the thread length. L and D can be expressed as functions of θ with constant parameters n and b,

$$L = b\cos\theta, \tag{5}$$

$$D = \frac{b\sin\theta}{n\pi}. \tag{6}$$

The volume of the cylinder is

$$V = \frac{1}{4}\pi D^2 L = \frac{b^3}{4\pi n^2}\sin^2\theta\cos\theta. \tag{7}$$

So, from equ. 4b, F can be expressed as a function of P' and θ,

$$F = -P'\frac{dV}{dL} = -P'\frac{dV/d\theta}{dL/d\theta} = \frac{P'b^2(2\cos^2\theta - \sin^2\theta)}{4\pi n^2} = \frac{P'b^2(3\cos^2\theta - 1)}{4\pi n^2}, \tag{8a}$$

which is equivalent to

$$F = \frac{\pi D_o^2 P'}{4}(3\cos^2\theta - 1) \tag{8b}$$

where $D_o = b/n\pi$, is the diameter when θ equals 90°, which is the same form used in Schulte's paper (1961).

The tension is thus linearly proportional to the pressure, and is a monotonic function of the braid angle ($0° < \theta < 90°$). The maximal shortening will be reached when $F = 0$, that is, $\theta = 54.7°$.

The physical non-ideality of the actuator will be considered while analyzing the experimental results later.

2) Dynamic testing machine

For the following experiments, a testing system capable of producing and recording desired patterns of the tension, length, and pressure of the actuator was built (Fig. 2). The system consists of five major hardware sub-systems and five major software sub-systems.

The hardware includes 1) an IBM compatible personal computer (PC, with 16 MHz 386SX), which executes the software and supports parallel bus for extensive hardware circuits, 2) PC extension bus interface and timer circuit, which supports programmable timing (with 1 μs resolution), interrupt signal, and any necessary bus buffering and address decoding, 3) analog sub-system, consisting of pressure sensors (6.8 bar max.), strain gauge force sensors (100 N max.), filters, amplifiers, and 8-bit A/D, D/A converters, which supports analog data I/O, 4) motor-position sensor sub-system, consisting of a 1/4 horse power DC motor, pulse-width-modulation power amplifier (± 24 A max. current), an optical angular position incremental encoder (1600 steps per revolution), a 24-bit decoder, and a pulley (ϕ 4 cm), which supports position control and force control (with above force sensor), and 5) pneumatic parts, including a pressure regulator (10 bar max.), an electro-valve (Festo proportional pressure regulator MPP-3-1/8, 10 bar max.), two gas accumulators (3 in^3 and 10 in^3), and flexible tubing (ϕ 1/8"). There is also a testing frame (12"w × 20"h × 8"d) to mount the mechanical parts, sensors, and the actuator.

The software includes 1) interface and timer configuration routines to implement timing and interrupt setting, 2) interrupt service routines to implement real-time waveform generating, data recording, and software feedback control at 1 kHz updating rate of all I/O channels (5 kHz max.), 3) user interface to interpret and execute user commands, and to prompt and echo system status and

messages, 4)waveform display to monitor testing results, and 5) disk data handler to load control waveform from, and to save response waveform to, disk. Most programs are written in C, and the rest are in assembly language.

By utilizing different combinations of the I/O channels and software settings, the system can performs a variety of testing conditions, such as constant pressure testing, isometric testing, isotonic testing, and pneumatic circuit testing, etc.

3) Quasi-static and dynamic experiments

Since there is no analytical solution to describe biological muscle tension-length-activation relationship, a variety of configurations have been chosen to illustrate part of this relationship, such as static tension-length relation under constant activation level (Gordon et al. 1966), isometric to isotonic quick release experiment (Gasser and Hill 1924), isokinetic experiment (Gasser and Hill 1924, Levin and Wyman 1927), isometric tension in response to activation (Burke et al. 1976, Chou and Hannaford 1992), etc. Notice that the activation is always an input to muscle mechanics, and either one of the other two quantities (tension and length) may be input or output. The pressure of the actuator is analogous to the activation level and will initially be thought of as an input to the actuator, which will be held as constant as possible in these experiments in order to minimize the effects of the pressure dynamics and thus simplify the analysis.

Three types of actuators were tested in quasi-static experiments and one was also tested in dynamic experiments. The first one, with nylon shell, is 14 cm resting length, and 1.1 cm in diameter at 5 bar no load. The second one, with fiberglass shell, is 20 cm in length, 0.9 cm in diameter. And the third one, manufactured by Bridgestone, is 14.7 cm in length, 1.5 cm in diameter

In quasi-static experiments, first, the nylon shell actuator was tested. A set of low frequency triangular wave displacements (relative to resting length, L_0 = 14 cm) to best cover the linear tension regions corresponding to different pressure levels are selected as the input. The displacements are set to 1 Hz with large operating range (which yields the peak velocity about 0.5 L_0/s).

The pressure is set by a manual regulator to obtain six desired constant levels (0-5 bar relative). Due to 1) the volume change of the actuator with length change, 2) the gas viscosity in connection tubing, and 3) the regulator's output hysteresis, the measured pressure will increase when the actuator lengthens and will decrease when it shortens. In order to reduce the variation of the pressure, a 10 in^3 (164 cm^3) accumulator is connected to the regulator, and a 3 in^3 (49 cm^3) accumulator is connected directly to the actuator. As a result, the pressure variation was limited to less than 0.1 bar due to the large total capacity of the accumulators, and the pressure hysteresis is almost immeasurable due to the close position (to the actuator) of the second accumulator.

Both the measured pressure and the tension are shown in response to the displacements (Fig. 3a). By minimizing the effect of pressure variation, the hysteresis loop of the tension-length relationship is illuminated. The width and height of the loop is about 0.2-0.5 cm and 5-10 N respectively. Two further experiments were made to illustrate more features of the hysteresis.

First, the frequency of the displacement waveforms is reduced to 0.25 Hz, while the operating

range remains the same (which yields the peak velocity about 0.125 L_o/s). The result is almost identical to the previous case, which suggests that the tension-length behavior is velocity independent at low velocities. Second, the frequency is set to 1 Hz, while the operating range is reduced about half (Fig. 3b, solid lines). The tension rising paths remain the same (the rising "initial conditions" are the same), but the falling paths are different (The falling "initial conditions" are different due to the smaller operating range). Thus the width and height of the loop are reduced. This indicates the hysteresis is history dependent.

The procedures to obtain Fig. 3a were repeated for the other two actuators, and the results in the same format are shown in Fig. 3c and d. The stiffness, friction, and extensibility are quite different in the above three actuators.

In dynamic experiments, only the first actuator was tested. A set of middle to high frequency sinusoidal displacement waveforms (relative to zero tension length) with small operating range are applied. The pressure is set to relative 5 bar, and remains constant quite well in this condition (due to smaller length change). The frequencies and displacement range are designed to obtain 0.2-8.0 L_o/s peak velocity yet remain in the linear tension-length region. The viscous friction (damping force) if measurable, would be revealed by a hysteresis width which is a monotonic increasing function of the velocity. However, the results show that the width of the tension-displacement loop is very small and almost unchanged, except for a slight decrease at higher frequency (Fig. 4).

These results indicate that the velocity-independent hysteresis is most likely to be the Coulomb friction, which dominates the total friction of the actuator. The viscous friction is much smaller than Coulomb friction and thus immeasurable.

An attempt to reduce the Coulomb friction was performed by applying three types of lubricant (including "WD-40 stops squeaks", 10W-40 engine oil, and another kind of small machine oil) on the braided shell and bladder of the nylon actuator. The Coulomb friction was reduced only 10% by these measures. A special type of lubricant is probably required to reduce the friction of plastic-plastic contacts.

4) Simplified static model

Excluding the above Coulomb friction, a hypothetical static tension-length relation can be calculated including a correction for the wall thickness if desired (Fig. 5a to d). From equ. 8b, the tension is linearly proportional to the pressure, and is a monotonic function of the braid angle ($0° < \theta < 90°$). However, if the thickness (t_k) of the shell and bladder is considered, the relation becomes

$$V = \frac{1}{4}\pi (D - 2t_k)^2 L, \tag{9}$$

by plugging into equ. 4b,

$$F = -P'\frac{dV}{dL} = \frac{\pi D_o^2 P'}{4}(3\cos^2\theta - 1) + \pi P'\left[D_o t_k (2\sin\theta - \frac{1}{\sin\theta}) - t_k^2\right]. \tag{10}$$

This is more complex than equ. 8b.

The actuator can also be considered as a variable-stiffness elastic element, or a "gas spring",

where the tension is a function of the pressure and the length. Its stiffness ($K \equiv dF/dL$) is proportional to the pressure, and the stiffness-per unit pressure ($K_g \equiv dK/dP'$) approximates a constant within 10 to 14 cm length by simulation (Fig. 5e, K_g = 0.461 cm, or 4.61 N/cm·bar, with t_k = 0.0762 cm and D_o = 1.66 cm). So, fortunately, it can be linearized as

$$F = K_g P' (L - L_{min}) \tag{11}$$

where L_{min} is the theoretically possible minimum length (when $F = 0$).

Now, considering energy stored by the actuator in its bladder and shell, yields

$$F = K_g (P' - P_{th}) (L - L_{min}) + K_p (L - L_o) + nl(L) \qquad \text{if } P' > P_{th}, \text{ or} \tag{12a}$$

$$F = K_p (L - L_o) + nl(L) \qquad \text{if } P' \le P_{th} \tag{12b}$$

where P_{th} is the threshold for the pressure to overcome the radial elasticity of the bladder for expanding, K_p is the linearized equivalent parallel passive elastic constant for the shearing force of the bladder material and shell threads, and $nl(\cdot)$ is the non-linear term due to the non-perfect cylinder while the actuator is at its extreme length (Fig. 6a). The first two product terms in equ. 12a can be expressed as

$$F = K_g (P' - P_a) (L - L_{min}) + F_a \tag{13}$$

where $P_a = P_{th} - K_p/K_g$, and $F_a = K_p (L_{min} - L_o)$. To experimentally estimate these parameters, 10 points of hypothetical static tension-length-pressure pairs are sampled from above quasi-static results and fit into equ. 13 (Fig. 6b). This calculation gives K_g = 0.466 cm, P_a = 0.062 bar, L_{min} = 9.91 cm, and F_a = -16.0 N. Also, P_{th} and K_p can be estimated by knowing L_o = 14.0 cm, which yields P_{th} = 0.903 bar and K_p = 3.92 N/cm. Notice the K_g is very close to the theoretical value 0.461 cm. The non-linear term only becomes significant when the actuator is extremely short or extremely long, usually this is out of regular operating range, and will not be discussed further.

5) Quasi-static and dynamic characteristics

It has been shown that there is hysteresis in the tension-length cycle, and that the dominant friction is the frequency insensitive Coulomb friction, which is caused by the contact between the bladder and the shell, between the braided threads and each other, and the shape changing of the bladder. The history dependence makes the friction difficult to predict precisely, especially after the actuator is attached to artificial bones with curving shape. So, it is suggested to add a typical friction value (± 2.5 N, positive for lengthening, negative for shortening) to the hypothetical static equation (equ. 12a or 13 and 12b) if a simple friction model is sufficient.

Part II Pneumatic circuits

Since the McKibben actuator is driven by pneumatic power, it is important to understand some basic phenomena of the pneumatic dynamics in order to distinguish the factors of pneumatic circuit from those of the actuator.

1) Pressure dynamic experiments in pneumatic circuits

The most important state variables in a pneumatic circuit are pressure and mass flow. The pressure can be measured directly, and the mass flow can be derived from the changing of the pressure in an accumulator.

Two pressure dynamic experiments were made with simple pneumatic circuits as shown in Fig. 7a including an electro-valve, which produces a non-periodical pressure waveform, pneumatic tubing (ϕ 1/8", length 100 cm), which introduces gas viscosity, an accumulator, which behaves as a capacitor, and two pressure sensors, one at the connection of the electro-valve output and the tubing (P_1), and the other at the connection of the tubing and the accumulator (P_2). The configurations of the two experiments are similar except the volume of one accumulator is 164 cm^3 (10 in^3) and the other is 49 cm^3 (3 in^3). The experimental results of the pressure responses will be shown with simulation results later. The modeling is limited to the response of P_2 to P_1, which includes the pneumatic characteristics of the tubing and the accumulator. However, the modeling of the electro-valve is not covered, because it is too complex to obtain an accurate yet simple model.

2) Lumped-parameter models of pneumatic circuits

To analyze a pneumatic circuit (even as simple as the above ones) is not easy in fluid dynamics. There are at least three reasons to explain that. First, it is a distributed-parameter system. The state variables are not only functions of time, but also functions of space, alternatively, there are infinite number of discrete state variables theoretically. Second, it is very geometry sensitive. All of the time-varying boundary conditions must be met to solve the gas momentum equation (Menkes et al. 1988),

$$\frac{D\mathbf{v}}{Dt} = -\frac{1}{\rho}\nabla P + \nu\nabla^2\mathbf{v} + \frac{1}{3}\nu\nabla(\nabla\cdot\mathbf{v}) + \sum\mathbf{F}, \tag{14}$$

and the energy equation,

$$\frac{\rho D(u+\mathbf{v}^2/2)}{Dt} = \nabla\cdot P\mathbf{v} + \rho\sum\mathbf{F}\cdot\mathbf{v} + \nabla\cdot k\nabla T + \sum Q, \tag{15}$$

$$\text{with } \frac{D}{Dt} \equiv \frac{\partial}{\partial t} + \mathbf{v}\cdot\nabla, \tag{16}$$

where ∇, gradient operator, $(\nabla\cdot)$,divergence operator, (∇^2), Laplacian operator, $\mathbf{v}$, gas velocity, ρ, density, P, pressure, ν, kinematic viscosity, F, any body force, u, internal energy, k, thermal conductivity, T, temperature, and Q, any other energy-transfer mechanism. Third, as the flow velocity rises, turbulent flow gradually takes over laminar flow. After that, it is impossible to obtain an analytical solution, and the system can only be solved by some powerful simulation program for a period of time.

The computation time will be of greater concern as the number of the actuators (and the pneumatic circuits) is increased in an application system. Lumped-parameter models with few parameters and few state variables can best meet this requirement. In the following, three models are described in the order of complexity as well as accuracy.

In the first model, two node pressures (P_1 and P_2, absolute) are the only state variables (as "effort" or voltage). The mass-flow (w) through each node (as "flow" or current) can be derived from these states with the parameters. The gas viscosity caused by the tubing (and the connections) is modeled as a linear resistor (R), and the accumulator as a linear capacitor (C) (Fig. 7b). By ignoring the volume of the tubing, there are the relations:

$$\frac{P_1 - P_2}{\mathrm{R}} = w, \tag{17}$$

$$w = \mathrm{C}\frac{dP_2}{dt}, \tag{18}$$

which yield

$$P_1 - P_2 = \mathrm{RC}\frac{dP_2}{dt}, \text{ or} \tag{19a}$$

$$\frac{P_2}{P_1} = \frac{1}{1 + s\mathrm{RC}} = \frac{1}{1 + s/\omega_c} \tag{19b}$$

after Laplace transformation, where s is the Laplace variable, and $\omega_c = 1/\mathrm{RC}$, the cut-off frequency. This is a linear low-pass-filter response with only one parameter (ω_c). A simulation of this model (equ. 19b with ω_c optimized to 4.0π, and rms. error = 0.19 bar) showed that the pressure rising speed (P_2, in response to P_1) in the model was faster in the low pressure situation and slower in the high pressure situation than the measured data. This indicates a linear resistance model cannot describe the real system very well.

In order to choose the most appropriate way to add non-linearity to the resistance, some phenomena of fluid dynamics must be considered: 1) gas resistance is more likely to be a function of gas velocity than a function of mass flow, 2) while in low gas velocity, gas tends to form laminar flow, and the resistance force is approximately proportional to the velocity, and 3) while in high gas velocity, gas tends to form turbulent flow, and the resistance force is approximately proportional to square of the velocity (see "friction factor" diagram, Moody 1944). These suggest a second power polynomial function of gas velocity should be able to appropriately describe the resistance.

In the second model, the resistance is modeled as

$$P_1 - P_2 = \mathrm{R}_1\left(\frac{w}{\rho_t A_t}\right) + \mathrm{R}_2\left(\frac{w}{\rho_t A_t}\right)^2 \tag{20}$$

where A_t is effective cross-section area of the tubing and connectors, R_1 and R_2 are constant and will be determined experimentally, and ρ_t is gas density inside the tubing,

$$\rho_t = \frac{P_t}{RT} \approx \frac{(P_1 + P_2)/2}{RT} \tag{21}$$

where R is gas constant per unit mass, T, temperature, and P_t is the average absolute pressure inside the tubing and is approximated to $(P_1 + P_2) / 2$.

The capacitance, C, is the same as in equ. 18, and $w \equiv dm/dt$, yields

$$\mathbf{C} = \frac{dm/dt}{dP_2/dt} = \frac{dm}{dP_2} \tag{22}$$

where m is gas mass in the accumulator. These experiments are a kind of gas "free expansion" from high pressure source into constant volume container, which is an isothermal process. Thus, $\mathbf{C}$ can be derived from the volume of the accumulator (V) and ideal gas equation,

$$PV = mRT, \tag{23}$$

by substituting P_2 for P and using equ. 22,

$$\mathbf{C} = \frac{V}{RT}. \tag{24}$$

By utilizing equ 18, 20, and 21, the accuracy of the simulation results are greatly improved (Fig. 8a and b), and $\mathbf{R}_1$ and $\mathbf{R}_2$ are optimized for each V.

The second model is very accurate, however, it should be noticed that the value of $\mathbf{R}_1$ and $\mathbf{R}_2$ for two circuits with different capacity change a lot after optimization. This means the model is not robust enough to handle the variable parameter situation. Also, when viewed with an expanded time scale, the simulation response leads the measured response by approximately 4 ms. This may suggest gas inertia should be considered in addition to non-linear viscosity (Fig. 7c).

The third model extends the second one by including the consideration of gas inertia ($\mathbf{L}$),

$$\Delta P = \mathbf{L}\frac{dw}{dt} \tag{25}$$

where ΔP is the pressure difference caused by inertial load. Converting Newton's first law,

$$F = d(m\mathbf{v})/dt \tag{26}$$

where F, force, m, mass, and $\mathbf{v}$, velocity, into pneumatic form, yields

$$A_t\Delta P = \frac{d(\rho_t A_t l_t \mathbf{v})}{dt} \tag{27}$$

where l_t is effective length of the tubing and connectors, and $\mathbf{v}$ is gas velocity. Also,

$$w = \rho_t A_t \mathbf{v}, \tag{28}$$

substitutes into equ. 27, giving

$$A_t\Delta P = \frac{dw}{dt} l_t, \tag{29}$$

with equ. 25, we obtain

$$\mathbf{L} = \frac{l_t}{A_t}. \tag{30}$$

Equ. 20 now should be modified into

$$P_1 - P_2 = \mathbf{R}_1\left(\frac{w}{\rho_t A_t}\right) + \mathbf{R}_2\left(\frac{w}{\rho_t A_t}\right)^2 + \mathbf{L}\frac{dw}{dt}. \tag{31}$$

By utilizing equ. 18, 21, and 31, the simulation results are shown in Fig. 9a and b. $\mathbf{R}_1$ and $\mathbf{R}_2$ now are optimized for the experiment with 10 in^3 accumulator, and without changing those values, applied to the 3 in^3 accumulator. For both accumulators we obtain very good accuracy with the same $\mathbf{R}_1$ and $\mathbf{R}_2$ and a slight improvement on the second model in terms of rms. error. Since the second model could only be fit to the two accumulators by re-optimizing $\mathbf{R}_1$ and $\mathbf{R}_2$, this model is a significant improvement. Also, the 4 ms lead in the simulation responses of the second model disappears. This illustrates that the robustness and accuracy of the model are improved by adding a simple inertia term.

Part III Isometric and isotonic experiments

In these two series of experiments, some characteristics related to both the actuator and gas dynamics will be demonstrated. These will give valuable information about the timing of the response waveform and the power capability of the system. For both series, particular patterns of control voltage are input to the electro-valve to generate dynamic pressure waveforms.

1) Isometric experiments

In these experiments, without using the motor, the actuator is fixed at the end to a stiff metal plate. The tension is recorded in response to a square wave (steps) control voltage, and the pressure recording is also shown for reference (Fig. 10). The delay time from the control voltage stepping to the pressure rising is about 5 ms, purely due to the delay of the valve. From the rise of pressure to the rise of tension is about 7 ms, mostly because it takes time for the pressure to overcome the threshold (P_{th}). The tension rising time (0 to 90%) is 30 ms for the full range step and 15 ms for the half range step, and the falling time (100% to 10%) is 53 ms and 30 ms respectively, these are limited by the maximum flow rate of the valve and the gas viscosity of the tubing (and connectors).

2) Isotonic experiments

In these experiments, closed loop control of the tension is performed by feeding back the measured tension to the motor drive. Three different frequency triangular waveforms are applied to the valve control voltage, and three different constant load levels are selected for the controlled tension. The pressure, shortening (negative displacement), and measured tension of selected typical results are shown in Fig. 11. It is evident that the measured tension has some variation due to limited capability of the motor sub-system and the bandwidth of the feedback. However, the positive work and power can still be calculated by numerically integrating the product of tension and positive shortening velocity. This gave the work per each shortening of 0.45 J, average power of 0.9 W, and peak power of 3.8 W at 10 N load-1 cycle per second, or the work per each shortening of 1.4 J, average power of 14 W, and peak power of 33 W at 50 N load-5 cycle per second. These values are for reference but do not represent the maximum capability of the actuator. The maximum power is mostly limited by the maximum pressure of the gas source, the maximum flow rate of the valve, and the gas viscosity inside the pneumatic circuit.

Part IV Energy conversion and efficiency

Energy efficiency is an important factor of an actuator. In order to estimate the energy efficiency of the actuator, several specific simulations will be introduced. This will also illustrate under what condition the higher efficiency may be obtained.

According to thermodynamics, mechanical energy is transformed into gas internal energy or heat when gas is compressed, and gas internal energy or heat is transformed back to mechanical energy when gas is expanded (except free expansion). In the following, a quantitative analysis of energy conversion in a pneumatic system with the nylon shell McKibben actuator will be classified into 3 different conditions: 1) quasi-stationary, constant pressure maximal shortening, 2) quasi-stationary, isotonic shortening, and 3) constant pressure isotonic shortening. For each condition, the process of energy conversion will also be separated into several steps in each cycle.

In general, the actuator can produce positive net mechanical work if it shortens at higher pressure under larger tension and lengthens at lower pressure under smaller tension (if the tension in shortening and in lengthening is the same, there will be no net work produced). This cycle can be expressed as five steps: 1) prepare the high pressure gas source, 2) shorten under high tension, 3) exhale, 4) lengthen under low tension, and 5) inhale for the next cycle. These steps will be specified for each condition as following:

1) Quasi-stationary, constant pressure maximal shortening condition

In this condition, the whole cycle, except exhaling, is assumed to be processed quasi-stationarily. This will eliminate any unnecessary energy loss, and will also make the isothermal assumption very reasonable. In addition, a hypothetical compressor with piston and inhale/exhale valves will be invoked to calculate the energy for preparing the high pressure gas source, which is assumed to connect with the actuator through a zero-volume tubing.

At the beginning of each cycle, the actuator is initially stretched at zero relative pressure by a tension against the passive elasticity of the actuator, and there is a certain amount of gas inside the compressor at environment pressure (point A in Fig. 12a and b).

The volume (V, variable) in Fig. 12a represents the total volume of gas inside the compressor plus the initial volume of the actuator (V_2, constant, at initial length L_2, constant). And the absolute pressure (P, variable) represents the gas pressure inside the compressor and the actuator. On the other hand, the length (L, variable) in Fig. 12b represents the length of the actuator bladder, and the tension (F, variable) represents the actuator tension at specific length and pressure.

In step 1, the pressure is increased by compressing the gas inside the compressor, while keeping the actuator isometric by increasing the tension accordingly (A to B). In step 2, let the actuator shorten as much as possible at constant pressure (until the tension becomes zero; B to C). In step 3, exhale the gas into environment (C to D). In step 4, re-stretch the actuator to its initial length (D to A in Fig. 12b). Finally, in step 5, inhale the certain amount of gas from environment into the compressor (D to A in Fig. 12a), and return to the initial condition.

In order to analyze this cycle, there are several constants must be introduced: V_i, total initial

gas volume, V_1, the maximally shortened actuator volume, P_o, the environment pressure, and P_h, the high pressure while shortening, L_o, the actuator resting length, L_1, the maximally shortened length, L_2, the initial stretched length, F_{2min}, the passive elastic tension at length L_2 and pressure P_o, and F_{2max}, the tension at length L_2, pressure P_h, and friction F_{cf}.

The mechanical energy applied by the piston to the gas in step 1 is:

$$W_{01} = -\int_{V_i}^{V_1} (P - P_o)\, dV = -\int_{V_i}^{V_1} P dV - P_o (V_i - V_1), \tag{32}$$

by utilizing the ideal gas equation (equ. 23),

$$PV = mRT = P_o V_i = P_h V_1, \tag{33}$$

giving

$$W_{01} = -P_h V_1 \int_{V_2}^{V_1} \frac{dV}{V} - P_o V_i \left(1 - \frac{P_o}{P_h}\right) = P_h V_1 \left(\log \frac{P_h}{P_o} - 1 + \frac{P_o}{P_h}\right), \tag{34}$$

which is a function of P_h and V_1. However, the maximally shortened length L_1 and V_1 are determined only by P_h. So W_{01} can be represented as a function of P_h only. To estimate L_1, the linearized tension-length-pressure equation as described in equ. 13 is solved by assigning $F = F_{cf}$ (F_{cf} is the estimated Coulomb friction), $P' = P_h - P_o$, and $L = L_1$, thus

$$L_1 = L_{min} + \frac{F_{cf} - F_a}{K_g (P_h - P_o - P_a)}. \tag{35}$$

And to estimate V_1 based on the same linearized model, equ. 4b is applied reversely with considering the offsets (pressure threshold and passive elasticity), which becomes

$$\frac{dV}{dL} = -\frac{dF}{dP'}, \tag{36}$$

$$\frac{d^2V}{d^2L} = -\frac{d^2F}{dLdP'} = -K_g, \tag{37}$$

$$V = -\iint_L K_g d^2L = -\frac{K_g}{2} (L - L_o)^2 + a_1 (L - L_o) + a_2, \tag{38a}$$

with conditions: $V_{L=L_o} = V_o$, and $(dV/dL)_{L=L_{min}} = 0$, yields

$$V = -\frac{K_g}{2} (L - L_o)^2 - K_g (L_o - L_{min})\, (L - L_o) + V_o. \tag{38b}$$

And V_1 is obtained by substituting L_1 for L.

The work input by the piston in step 2 is,

$$W_{12} = (P_h - P_o)\, (V_1 - V_2), \tag{39}$$

which is also a function of P_h only.

The net work output by the actuator is equivalent to the area of tetragon ABCD in Fig. 12b,

$$W_a = \frac{1}{2}\left[(L_2 - L_1) F_{2max} - (L_2 - L_o) F_{2min} \right], \tag{40}$$

which is a function of L_1, therefore, is a function of P_h only.

Now, the efficiency of energy conversion can be calculated as

$$E_a = \frac{W_a}{W_{01} + W_{12}}, \tag{41}$$

which shows the maximum efficiency is about 0.3 at P_h = 5 bar relative pressure, decreases slowly for higher pressure, and decreases to zero very fast for lower pressure when the pressure approaches the threshold P_{th} (Fig. 12c). Notice that W_a is always less than W_{12}, and W_{01} is wasted totally when exhaling (free expansion).

2) Quasi-stationary, isotonic shortening condition

In this condition, the whole cycle, except exhaling, is assumed to be processed quasi-stationarily. The initial condition is the same as the previous one (point E in Fig. 13a and b, except different initial gas volume). Then, in step 1, the pressure is increased by compressing the gas inside the compressor, while keeping the actuator isometric by increasing the tension accordingly (E to F). In step 2, let the actuator shorten isotonically while continuing to increase the pressure (F to G). In step 3, exhale the gas into environment (G to H). In step 4, re-stretch the actuator to its initial length (H to E in Fig. 13b). Finally, in step 5, inhale the certain amount of gas from environment into the compressor (H to E in Fig. 13a), and return to the initial condition.

The variables and constants in Fig. 13a and b have the same meaning as in Fig. 12a and b. In addition, the constant V_3 indicates the volume of the actuator at length L_3, and F_2 is the isotonic tension which is set to $(F_{2max} + F_{2min})/2$ (this may obtain close to maximum output work with the same P_h).

Due to the complexity of analytical approach for this isotonic case, only one value of the efficiency is calculated numerically by integration of the two loops with P_h at 5 bar relative pressure. This obtains E_b = 0.22.

3) Constant pressure isotonic shortening condition

In step 2 of the second condition, the pressure is increased according to the isotonic requirement while the actuator is shortening, however, the compressor may not be so "programmable" to produce the pressure pattern, or, this "hypothetical" compressor may be replaced by a valve and supply. So, instead of moving from point E through F to G in the prior condition, the *P-V* states go from point E through F' to reach P_h while compressing, then go to G with constant pressure (Fig. 13a). The additional energy (area FF'G) is wasted by the pressure-reducing mechanism of the valve and the gas viscosity in the pneumatic circuit under non-stationary condition. This yields the efficiency, E_c = 0.20.

Efficiencies improvement

The above efficiencies can only be obtained without any additional energy loss in the system

(e.g., loss by non-isothermal conditions, or friction between the compressor cylinder wall and piston). Therefore the efficiency in a practical implementation should be expected even lower. Fortunately, there is a feasible way to improve it. That is to inhale / exhale gas from / to an accumulator with internal pressure equal to the threshold ($P_{th} + P_o$ absolute) instead of from / to environment (P_o absolute). This will not effect the output work done by the actuator, but will reduce the input work done by the piston, which is equivalent to reducing the area from ABCD of Fig. 12a to A'BCD', and from EFGH of Fig. 13a to E'FGH', respectively. For the case $P_h = 5$ bar relative, the new value of E_a is 0.49, E_b is 0.39, and E_c *is* 0.32. This is much higher than before.

Summary

In part I, we have measured the mechanical characteristics of the McKibben muscles (the actuators), which behave like a variable-stiffness elastic element with velocity-insensitive friction. The stiffness is mostly dependent on the internal gas pressure. However, in order to produce tension, the pressure must be higher than a threshold to overcome the radial elasticity of the bladder. Also, a piecewise-linear, static model of the McKibben muscle has been derived. The format of the model was simplified and linearized from theoretical results, and the parameters were optimized with experimental data. The friction, although insensitive to velocity, is history dependent, and thus is difficult to model. A constant Coulomb friction was suggested and integrated into the static model to obtain a dynamic model.

The pressure dynamics of a simple tubing-accumulator pneumatic circuit and three lumped parameter models were measured and simulated in part II. The first model is a linear resistor-capacitor model (first-order dynamics), which is too simple to describe the real system. The second one consists of a second-power-polynomial non-linear resistive element and a linear capacitive element (first-order dynamics), which can produce much more accurate results. However, it is not robust enough when the parameters are changed. The third one, by adding linear inertial term into the previous model, forms a second-order dynamic model. Using this model, both the accuracy and the robustness were greatly improved, and the complexity of the model is still much simpler than to solve the fluid (gas) dynamic equations.

In part III, the integration of the actuator dynamics and the pneumatic circuit were demonstrated by isometric experiments and isotonic experiments. Typical values of shortening power and works per cycle were given for reference, but these are not the upper limits. The maximum average shortening power is mostly limited by the pneumatic circuit and the gas source.

By applying the actuator's mechanical model built in part I, the energy conversion and efficiency based on gas dynamics and thermodynamics was evaluated in part IV. It has been shown that the efficiency is dependent on the actuator's mechanical cycle and the compressor's pneumatic cycle, and the value is within 0.32 to 0.49 at $P_h = 5$ bar. However, depending on real cases, there are specific limitations for the tension-length and the pressure-volume relationships which are very likely to cause the maximum-efficiency cycle to be impossible to obtain. Also, additional pneumatic losses (viscosity in tubing, regulator, and valve) and mechanical losses (friction in compressor) will reduce the efficiency further more. The friction of the actuator has already been taken into account in the calculations.

Discussion

In the following, comparisons will be given between the McKibben muscles and biological skeletal muscles in terms of static properties, dynamic properties, and energy efficiencies. Selected properties of the supplementary pneumatic elements will also be evaluated.

1) Static properties: tension-length-activation relationships and output work

The general shape of the tension-length curve of the actuators is a monotonic increasing function of the length. For the tested nylon shell actuator, the tension reaches zero when the length is shorter than 0.75 L_o (L_o = 14 cm), and becomes very stiff when the length is longer than 1.1 L_o. Between these two points, the stiffness is about constant with a typical value of 23 N/cm (322 N/L_o) at 5 bar, and is approximately proportional to the pressure with some offset. The maximum tension is 110 N at 1.1 L_o and 5 bar. The integration of the tension within 0.75 to 1.1 L_o is 19 NL_o, which is the maximum output work per each mechanical cycle.

In order to calculate the stiffness and tension intensities per unit cross section area and the work per unit volume, we use the external cross section area at maximal shortening, because this is the maximum cross section area which the actuator should be allowed to occupy in a limb segment. For the nylon shell actuator, the cross section area is 0.95 cm^2 at 0.75 L_o, which yields the stiffness intensity of 340 N/$L_o cm^2$, the maximum tension intensity of 116 N/cm^2, and the work per cycle per unit volume of 0.20 J/cm^3.

The above properties of the other two actuators (fiberglass shell and Bridgestone) are listed in Table 1. The way that the threads form the external braided shell of the actuators influences most differences between the three actuators. The fiberglass shell actuator consists of a high thread density, thin threads, and large resting braid angle shell, which yields the largest 15% extensibility, lowest tension and stiffness intensities, and lowest work density. The nylon shell actuator consists of a low thread density, middle thickness threads, and middle resting braid angle shell, which yields the widest 35% dynamic range, highest work density, and smallest Coulomb friction. The Bridgestone actuator consists of a high thread density, thick threads, and small resting braid angle shell, which yields the narrowest 24% dynamic range, almost no extensibility, and the highest tension and stiffness intensities.

For biological muscles, the tension-length relation can be described by the "active tension" with a trapezoidal shape and the "passive tension" with increasing stiffness when stretched beyond a certain length. There may be a local maximum of the total tension if the increase of passive tension is less than the decrease of active tension to the length. The zero-tension lengths of the active tension are 0.64 and 1.8 L_o (frog striated muscle, Gordon et al. 1966), however, if we define the dynamic range of biological muscles by the non-negative-slope region of the active tension-length curve, then it is within 0.64 to 1.12 L_o. The maximum tension intensity is about 35 N/cm^2 (Guyton 1986, or 30 N/cm^2 from Gordon 1989), this yields the average stiffness intensity of 73 N/$L_o cm^2$, and the work per cycle per unit volume of 0.13 J/cm^3 by numerically integrating the tension-length curve within the dynamic range.

In summary, the biological muscle can be stretched beyond its resting length much longer than

the actuators, but usually this is beyond the ordinary physiological operating region. Also, the biological muscle can shorten a little more than the actuators This is a major disadvantage of the actuators. On the other hand, the tension intensity of the actuators is much higher than biological muscles, this is a major advantage of the actuators and yields higher work density and stiffness intensity. Finally, to improve the match to biological muscle static properties, passive parallel and serial elastic elements, which exist in biological muscles, can be added into the actuators without difficulty.

2) Dynamic properties: tension-velocity relationships, power, and response time

The tension-velocity relation of the nylon shell actuator, if we do not count the viscosity of the pneumatic circuit, is dominated by a velocity-insensitive Coulomb friction, and the velocity-dependent viscous friction is immeasurable (below 8 L_o/s velocity at least), which yields a very high maximum velocity in theory. The measured power per unit volume is 1.1 W/cm^3 in average of half cycle and 2.65 W/cm^3 in peak. For the full activation step response, the total delay time in above experiments is 12 ms, the tension rising time is 30 ms, and the falling time is 53 ms.

On the other hand, the hyperbolic tension-velocity curve of biological muscles indicates the viscosity decreases when the velocity increases (Hill 1938), and there is no Coulomb friction reported. The typical maximum shortening velocity is 2 L_o/s for slow muscle and 8 L_o/s for fast muscle (Winters 1990) or 20 L_o/s for fast muscle (Gordon 1989). According to Hill's tension-velocity curve, the maximum peak power is about 0.1 $F_{max}v_{max}$ (McMahon 1984). Applying 35 N/cm^2 maximum tension intensity and 20 L_o/s maximum shortening velocity yields maximum peak power per unit volume of 0.70 W/cm^3 for skeletal muscle.

Obviously the tension-velocity relationship of the actuator is not similar to that of biological muscles. Fortunately, the viscous friction is very small and thus we can add some parallel viscous elements to simulate biological muscles. In addition, although the lubricants used in quasi-static experiments do not significantly reduce the Coulomb friction, there may be some other kinds of lubricant which are more effective. Finally, The response time of biological muscles, although are not given here, have very wide range, and can be shorter in fast muscles than in the actuator.

3) Energy efficiencies

The theoretical maximum energy efficiency of the nylon shell actuator is about 0.32 to 0.49. This seems higher than 0.2 to 0.25 of human muscles (Hill 1922, Guyton 1986). However, as mentioned before, the actual energy efficiency of the actuator will be lower due to additional non-ideal energy losses.

4) Supplementary pneumatic elements

Besides the above considerations, the properties of the supplementary pneumatic elements which are necessary in order to drive the actuator must be considered, too. The necessary elements include an electro-valve, tubing, and a high pressure gas source.

The Festo MPP-3-1/8 electro-valve used in above experiments is 0.8 kg in weight, 14.5x4.5x4.5 cm^3 in size, and it takes 0.95 A current at 18 V to get 600 l/min flow rate at 6.9 bar

input without load. Another valve we tested (Animate Systems SARCOS servovalves C100P/80) is 0.1 kg in weight, 8.3x1.9x1.9 cm^3 in size, takes 0.4 A at 5.8 V to get 23 l/min at the same conditions, the flow rate of the former is much higher with the costs of higher control energy and bigger size. The higher flow rate valve will shorten the system response time, and thus gives a closed loop controller more flexibility to remain stable. However, it is much heavier and bigger than the actuator. This will increase the total weight and size of the system, and also force the designer to avoid to put the valves on moving parts, thus long tubing must be used to connect each valve with each independent-controlled actuator. Also, the high control energy will reduce the energy efficiency of the whole system.

About the tubing, there may be many pieces of tubing, long and wrapping around, in a whole system. The gas viscosity inside tubing decreases while its diameter increases, however, its flexibility decreases at the same time. So, trade off exists between high flexibility, in order not to disturb movement, and low viscosity, in order not to slow down response.

In order to drive several actuators for many shortening-lengthening cycles, there must be a gas reservoir with very high pressure and acceptable volume if there is no additional energy source. This will waste a lot of energy to compress gas above necessary operating pressure while preparing the high pressure source and yields a very poor energy efficiency. On the other hand, a compressor with motor or engine may solve the poor energy efficiency problem, however, it may be heavy and noisy. Finally, a low pressure reservoir with heating chamber may obtain the highest efficiency since the heat is converted directly to actuator's mechanical energy, however, the gas may be so hot to damage the actuator and injure the user.

Conclusion and future work

The linearized mechanical model of the actuator and the lumped parameter model of the pneumatic system gave us simple yet accurate descriptions of the actuator and the pneumatic behaviors. Although no mechanical-pneumatic integrated model was shown, a model can be made by substituting the actuator for the accumulator, cascading the output of the pneumatic circuit model to the input of the actuator dynamic model, and adding a feedback pathway from the length of actuator to its volume (gas capacitance). This may analogous to the mechanical coupling of calcium ion concentration (or active state) in real muscle (Zahalak 1990, Gordon and Ridgway 1990). These models can be used in simulation of single or multiple actuator systems for design consideration.

The static mechanical features of the actuator are very similar to biological muscles, except the dynamic range is narrower and the tension intensity is much higher. Some parallel and serial elastic elements may be added to fine tune the passive elastic characteristics. On the other hand, some dynamic features may need to be modified to get even closer, for examples: use lubricant to reduce the Coulomb friction and add some viscous material to increase the viscous friction in order to fit the tension-velocity relationship. Propagation delay can be added if the response is faster than some biological motor unit.

The pneumatic system, which provides control and power to the actuator, however, still needs a lot of improvement, for example: we need to find a lighter valve with acceptable flow rate,

integrate the tubing into the muscle-bone assembly components to solve tubing length and wrapping problems, and find a light and quite gas source with reasonable energy efficiency. Beside the actuators performance, these are important problems which must be solved in order to implement a feasible muscle replacement system.

References

Burke R E, Rudomin P and Zajac F E (1976) The effect of activation history on tension production by individual muscle units. Brain Res. 109: 515-529

Chou C-P and Hannaford B (1992) Dual stable point model of muscle activation and deactivation. Biol. Cybern. 66: 511-523

Gasser H S and Hill A V (1924) The dynamics of muscular contraction. Proc. R. Soc. B 96: 398-437

Gavrilovic M M and Maric M R (1969) Positional servo-mechanism activated by artificial muscles. Med. & Biol. Engng. 7: 77-82

Gordon A M, Huxley A F and Julian F J (1966) The variation in isometric tension with sarcomere length in vertebrate muscle fibers. J. Physiol. 184: 170-192

Gordon A M (1989) Contraction in skeletal muscle. In: Textbook of physiology, vol 1: excitable cells and neurophysiology, chap 8, 21st edn. Seattle, Washington

Gordon A M and Ridgway E B (1990) Stretch of active muscle during the declining phase of the calcium transient produces biphasic changes in calcium binding to the activating sites. J. Gen. Physiol. 96: 1013-1035

Guyton A C (1986) Contraction of skeletal muscle. In: Textbook of medical physiology, chap 11, 7th edn

Hannaford B and Winters J M (1990) Actuator properties and movement control: biological and technological models. In: Multiple muscle systems, Winters J, Woo S (eds). Springer-Verlag, New York

Hill A V (1922) The maximum work and mechanical efficiency of human muscles and their most economical speed. J. Physiol. 56: 19-41

Hill A V (1938) The heat of shortening and the dynamic constants of muscle. Proc. R. Soc. B 126: 136-95

Levin A and Wyman J (1927) The viscous elastic properties of muscle. Proc. R. Soc. B 101: 218-243

McMahon T A (1984) Fundamental muscle mechanics. In: Muscle, reflexes, and locomotion, chap 1, Princeton University Press, Princeton, New Jersey

Menkes J, Cambel A B and Talbot L (1988) Gas dynamics. In: Fluid mechanics source book, Parker S P (ed). McGraw-Hill, New York

Moody L F (1944) Friction factors for pipe flow. Transactions of ASME. vol. 66

Schulte H F Jr (1961) The characteristics of the McKibben artificial muscle. In: The Application of external power in prosthetics and orthotics. National Academy of Sciences-National Research Council, Washington D. C.

Winters J M (1990) Hill-based muscle models: a system engineering perspective. In: Multiple muscle systems, Winters J, Woo S (eds). Springer-Verlag, New York

Zahalak G I (1990) Modeling muscle mechanics (and energetics) In: Multiple muscle systems, Winters J, Woo S (eds). Springer-Verlag, New York

Legends

Fig. 1 Geometry of actuator. Middle portion of the actuator is modeled as perfect cylinder with length L, diameter D. θ, angle between braided thread and cylinder long axis, n, number of turns of thread, and b, thread length. Relationship between above parameters is illustrated by triangle.

Fig. 2 Block diagram of dynamic testing machine.

Fig. 3 a to **d** Quasi-static experiments. **a** and **b** X-Y plots of experimental results for nylon shell actuator. Six pairs of curves are superimposed in plots: nearly horizontal curves, measured pressure-length, sloped curves, tension-length. Operating pressure in bar is printed just above each tension-length loop. Hysteresis direction is clockwise. **a** Large range, 1 Hz. **b** Small range, 1 Hz. **c** X-Y plot of experimental results for fiberglass shell actuator. **d** X-Y plot of experimental results for Bridgestone actuator.

Fig. 4 X-Y plot of dynamic sinusoidal responses. Results for 12 frequencies are combined together with shifting curves along displacement axis. Notice width of hysteresis is almost unchanged for peak velocity from 0.2 L_o/s (1 Hz) to 2.0 L_o/s (10 Hz). Hysteresis direction is clockwise.

Fig. 5 a to **e** Simulation results of nylon shell actuator's static characteristics as function of length. Dashed lines, results considering thickness of braided shell and bladder, solid lines, results without considering wall thickness.

Fig. 6 a and **b** Static model of actuator. **a** total tension is summation of active term, passive term, and non-linear term. **b** Parameters of linearized model are optimized with 10 tension-length-pressure sample points from experimental data of Fig. 3a. x, sampled pressure, +, sampled tension, o, simulation tension.

Fig. 7 a Pneumatic circuit configuration. **b** Circuit notation of lumped parameter model with capacity and viscosity. **c** Circuit notation of lumped parameter model with additional inertia.

Fig. 8 a and **b** Dynamic responses of pneumatic circuit with simulation results of non-linear viscosity model. Center lines, input pressure P_1, dashed lines, measured output P_2, solid lines, simulation output P_2. **a** With accumulator $V = 10$ in^3, $\mathtt{C} = 0.190$ g/bar, $\mathtt{R}_1 = 4.91\text{e-}6$ bar·s/cm, $\mathtt{R}_2 = 2.07\text{e-}8$ bar·s^2/cm^2, rms. error = 0.111 bar. **b** With accumulator $V = 3$ in^3, $\mathtt{C} = 0.057$ g/bar, $\mathtt{R}_1 = 4.50\text{e-}6$ bar·s/cm, $\mathtt{R}_2 = 2.61\text{e-}8$ bar·s^2/cm^2, rms. error = 0.132 bar.

Fig. 9 a and **b** Dynamic responses of pneumatic circuit with simulation results of additional inertia model. Center lines, input pressure P_1, dashed lines, measured output P_2, solid lines, simulation output P_2. $\mathtt{L} = 1.26\text{e-}3$ bar·s^2/g (= 126 cm^{-1}), $\mathtt{R}_1 = 4.91\text{e-}6$ bar·s/cm, $\mathtt{R}_2 = 2.07\text{e-}8$ bar·s^2/cm^2. **a** With accumulator $V = 10$ in^3, $\mathtt{C} = 0.190$ g/bar, rms. error = 0.107 bar. **b** With accumulator $V = 3$ in^3, $\mathtt{C} = 0.057$ g/bar, rms. error = 0.127 bar.

Fig. 10 Isometric step response experiments. Two sets of curves in response to two different amplitudes of control voltage steps are superimposed in plot. Upper lines, control voltage ratio,

dashed lines, valve output pressure, middle solid lines, actuator pressure, lower lines, tension.

Fig. 11 Isotonic triangular response experiments. Two typical results are shown at 1 cycle per second with 10 N and 50 N load respectively. Center lines, actuator pressure, dashed lines, tension, solid lines, shortening. Power is product of tension and shortening velocity.

Fig. 12 a to **c** Illustration of actuator's energy efficiency for quasi-stationary constant pressure shortening condition. **a** Pneumatic cycle of hypothetical compressor at P_h = 5 bar relative. Total input work is 8.86 J for ABCD cycle, and 5.50 J for A'BCD' cycle. **b** Mechanical cycle of actuator. Output work is 2.59 J (with 2.5 N Coulomb friction), which yields efficiencies are 0.29 and 0.49 respectively. **c** Energy efficiencies (E_a) as functions of high pressure level P_h. Lower traces, gas is exchanged from environment (ABCD cycle). Upper traces, gas is exchanged from an accumulator with absolute pressure $P_{th} + P_o$ (A'BCD' cycle). Solid lines, with 2.5 N Coulomb friction at shortening, dashed lines, without friction.

Fig. 13 a and **b** Illustration of actuator's energy efficiency for quasi-stationary isotonic shortening and constant pressure isotonic shortening conditions. **a** Pneumatic cycle of hypothetical compressor at P_h = 5 bar relative. Total input works are 5.79 J for EFGH cycle, 3.29 J for E'FGH' cycle, 6.46 J for EF'GH cycle, and 3.96 J for E'F'GH' cycle. **b** Mechanical cycle of actuator. Output work is 1.27 J (with 2.5 N Coulomb friction), which yields efficiencies are 0.22, 0.39, 0.20, and 0.32, respectively.

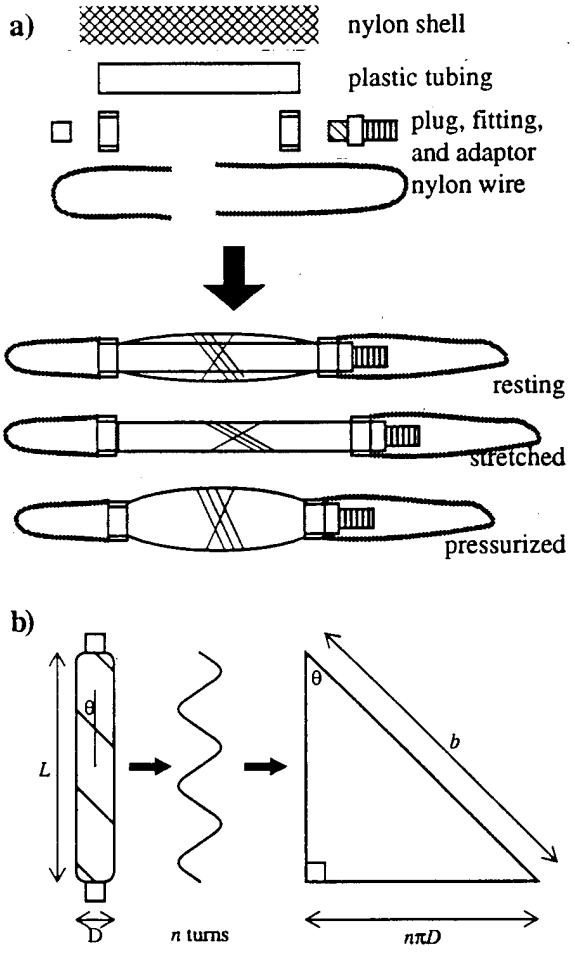
a)
nylon shell
plastic tubing
plug, fitting,
and adaptor
nylon wire
resting
stretched
pressurized
b)
θ
L
D
n turns
θ
b
nπD

Fig.1

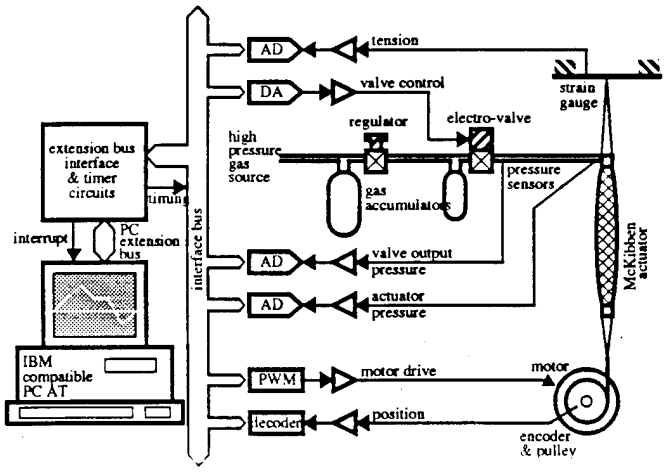
AD
tension
DA
valve control
strain gauge
regulator
electro-valve
high pressure gas source
extension bus interface & timer circuits
gas accumulator
pressure sensors
interrupt
PC extension bus
interface bus
AD
valve output pressure
AD
actuator pressure
McKibben actuator
IBM compatible PC AT
PWM
motor drive
motor
decoder
position
encoder & pulley

Fig.2

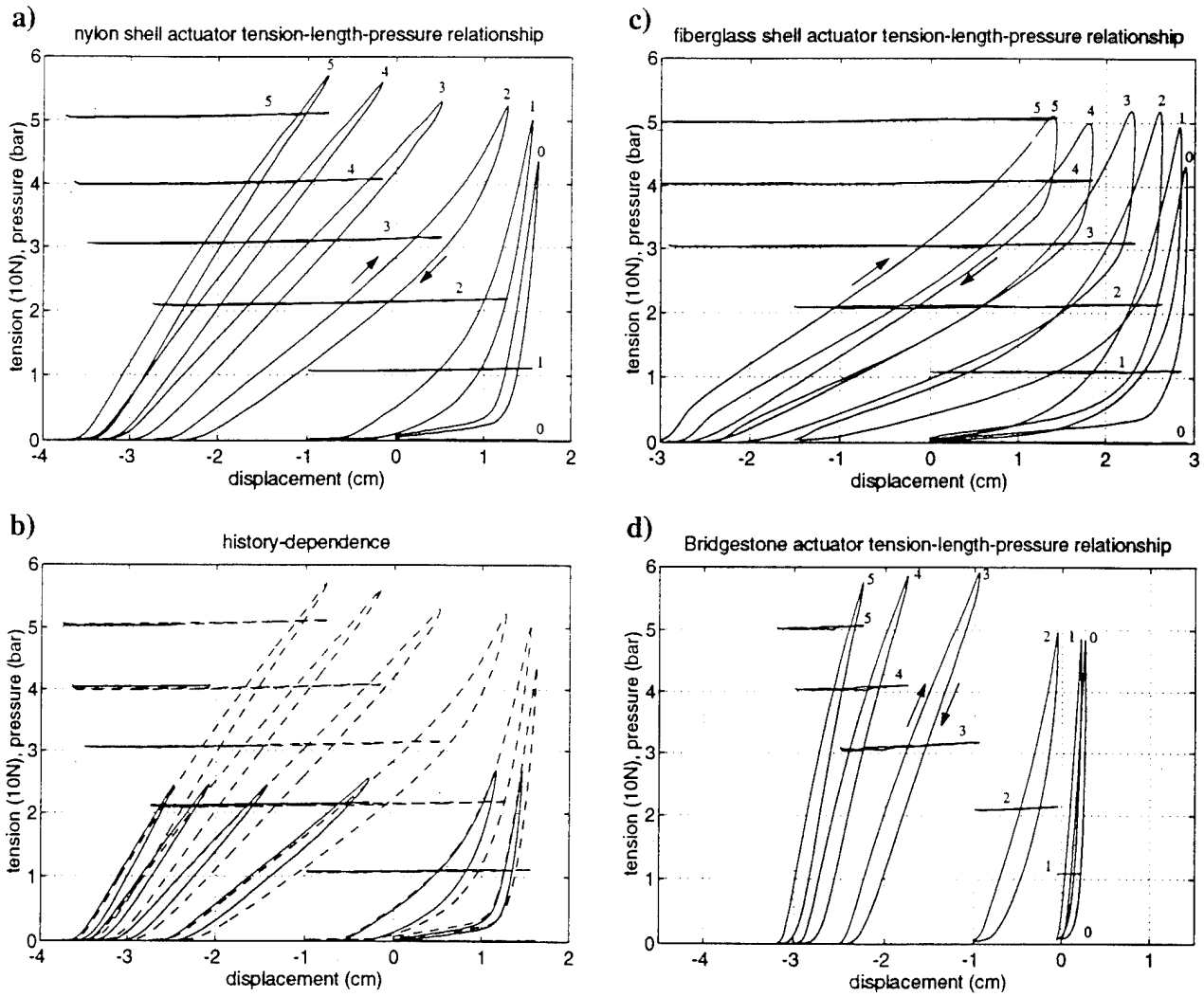
a)
nylon shell actuator tension-length-pressure relationship
tension (10N), pressure (bar)
displacement (cm)
c)
fiberglass shell actuator tension-length-pressure relationship
tension (10N), pressure (bar)
displacement (cm)
b)
history-dependence
tension (10N), pressure (bar)
displacement (cm)
d)
Bridgestone actuator tension-length-pressure relationship
tension (10N), pressure (bar)
displacement (cm)

Fig.3

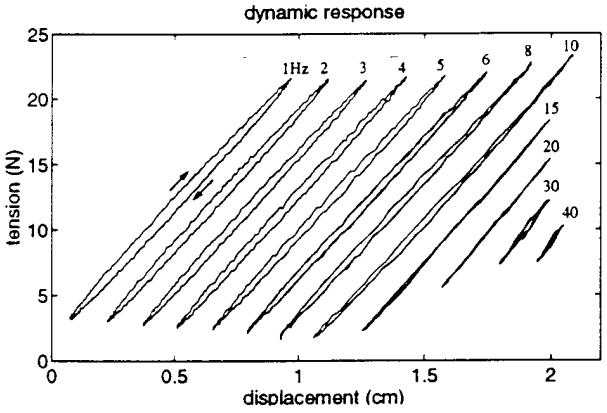

Fig.4

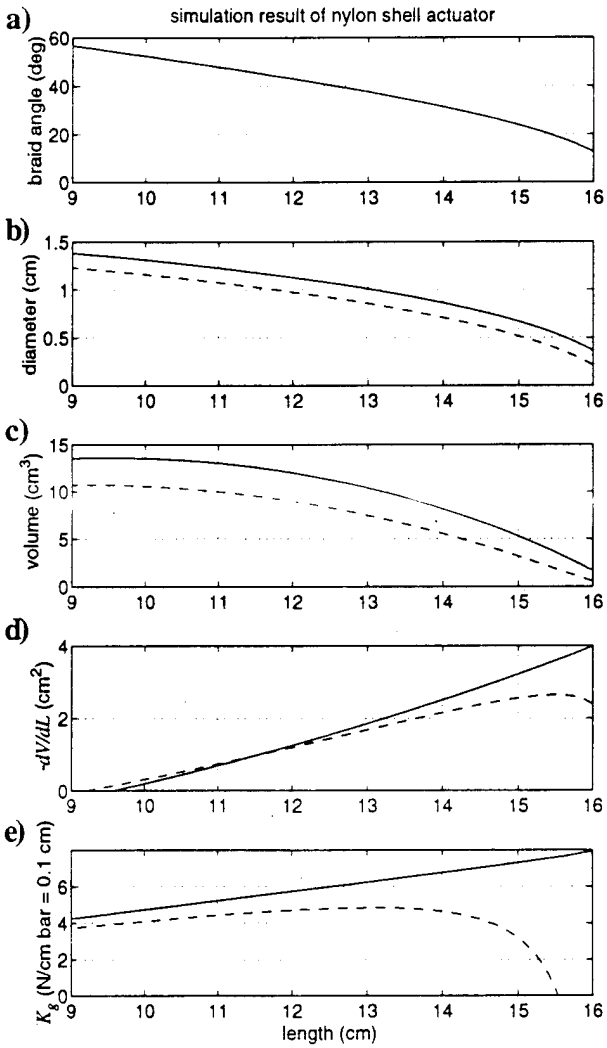

Fig.5

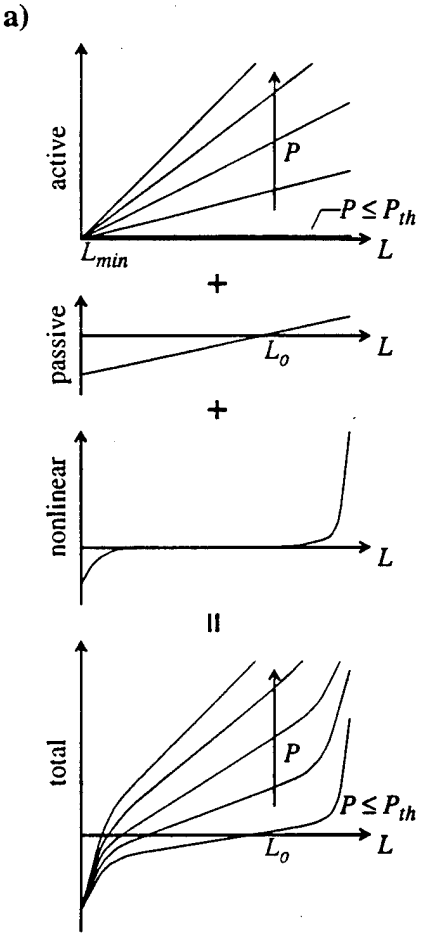

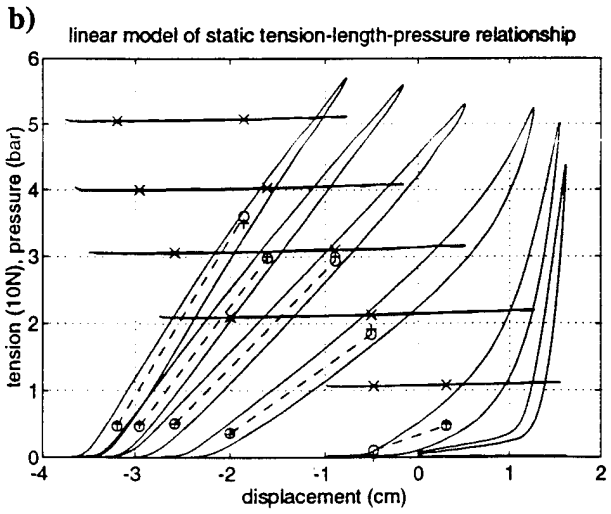

Fig.6

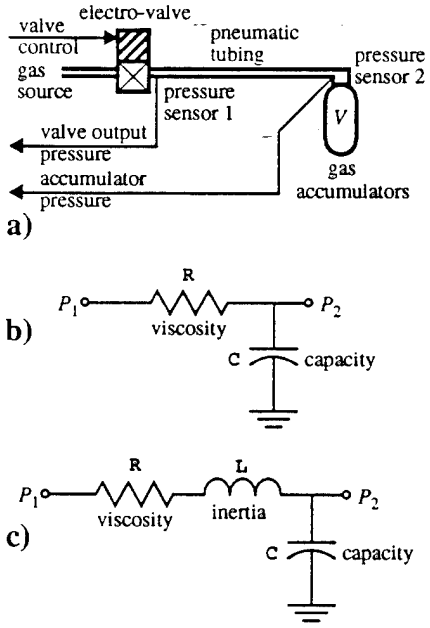

Fig.7

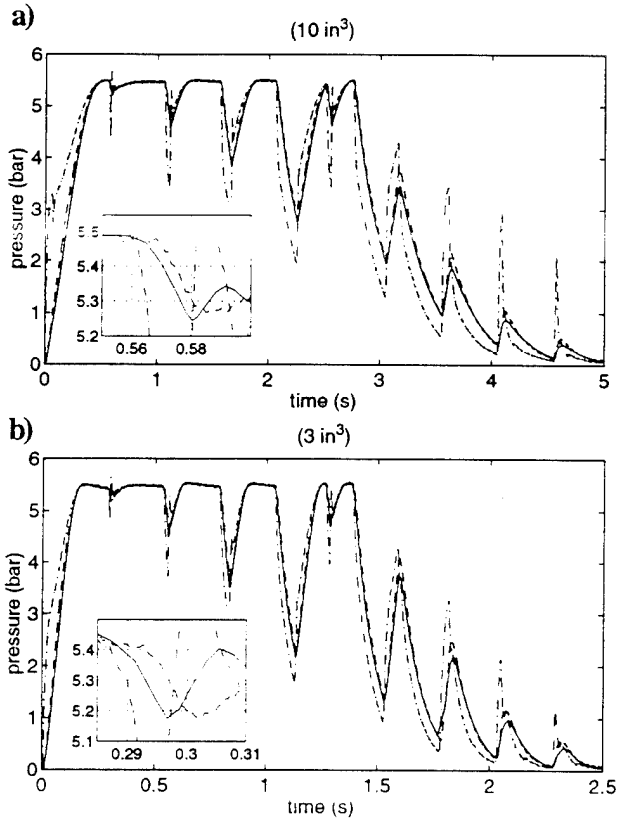

Fig.8

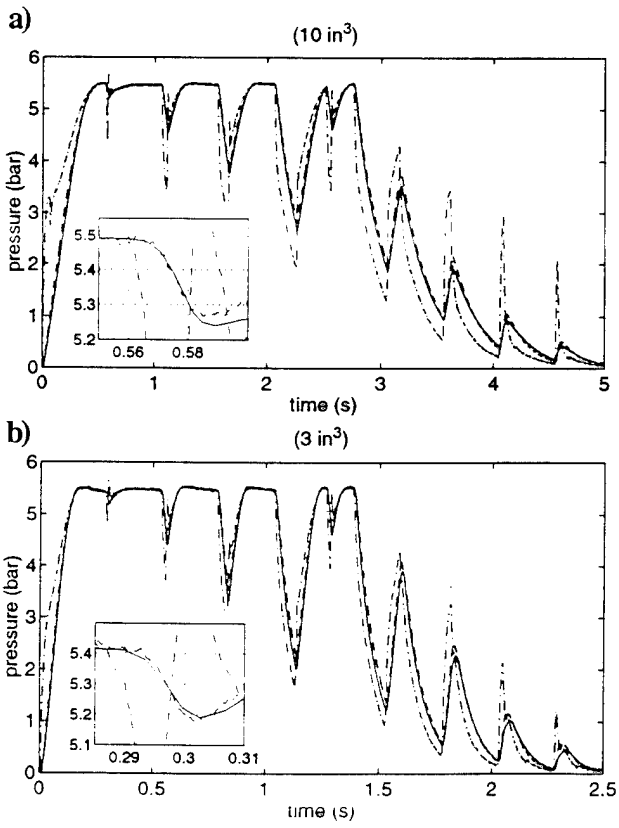

Fig.9

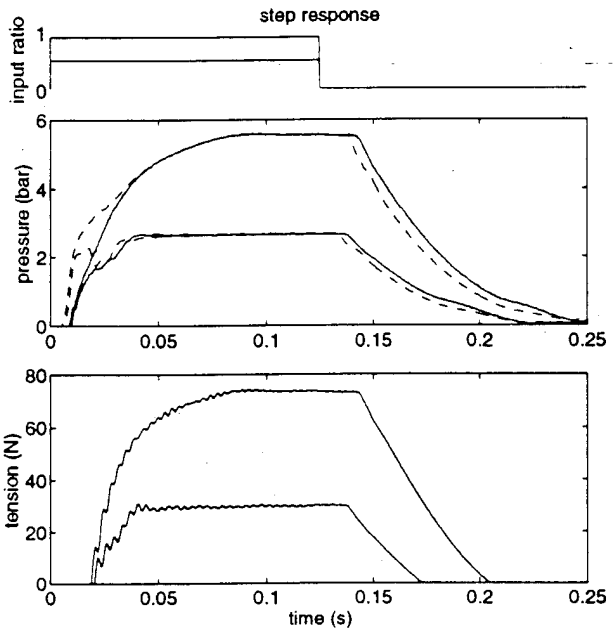
step response
input ratio
pressure (bar)
tension (N)
time (s)

Fig.10

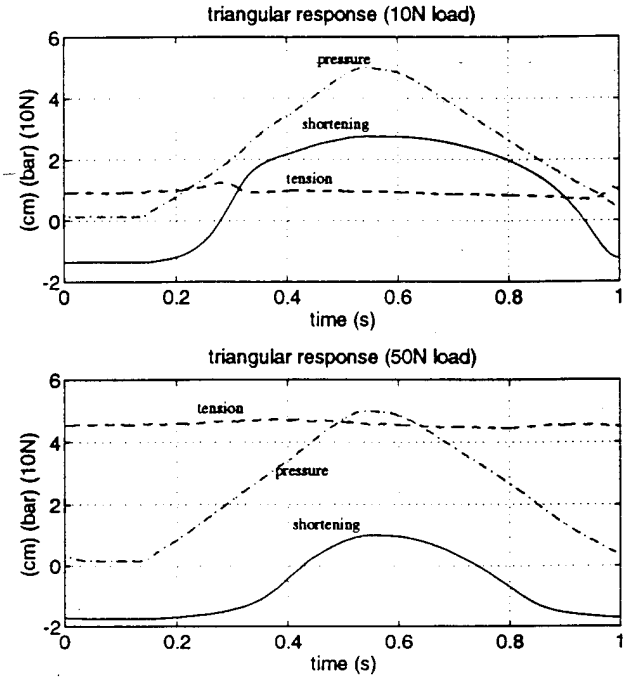
triangular response (10N load)
pressure
shortening
tension
(cm) (bar) (10N)
time (s)
triangular response (50N load)
tension
pressure
shortening
(cm) (bar) (10N)
time (s)

Fig.11

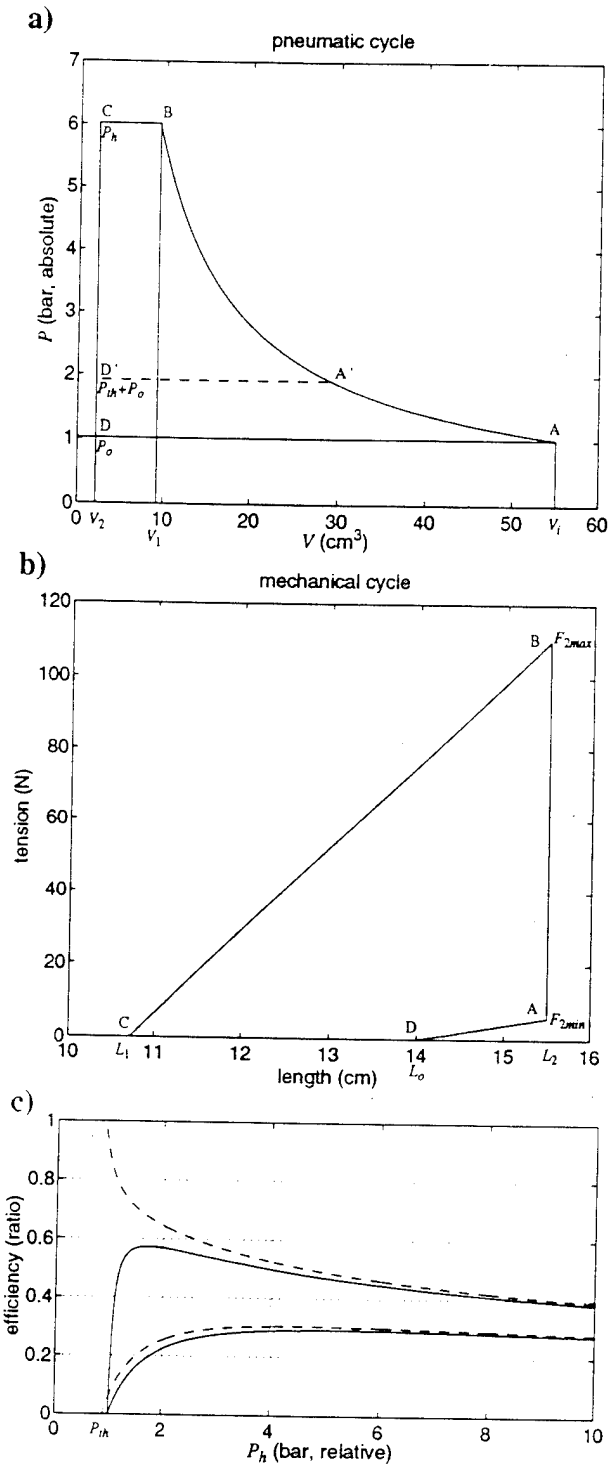
a)
pneumatic cycle
P (bar, absolute)
V (cm3)
C
B
A'
D'
D
A
b)
mechanical cycle
tension (N)
length (cm)
B
C
D
A
c)
efficiency (ratio)
Ph (bar, relative)

Fig.12

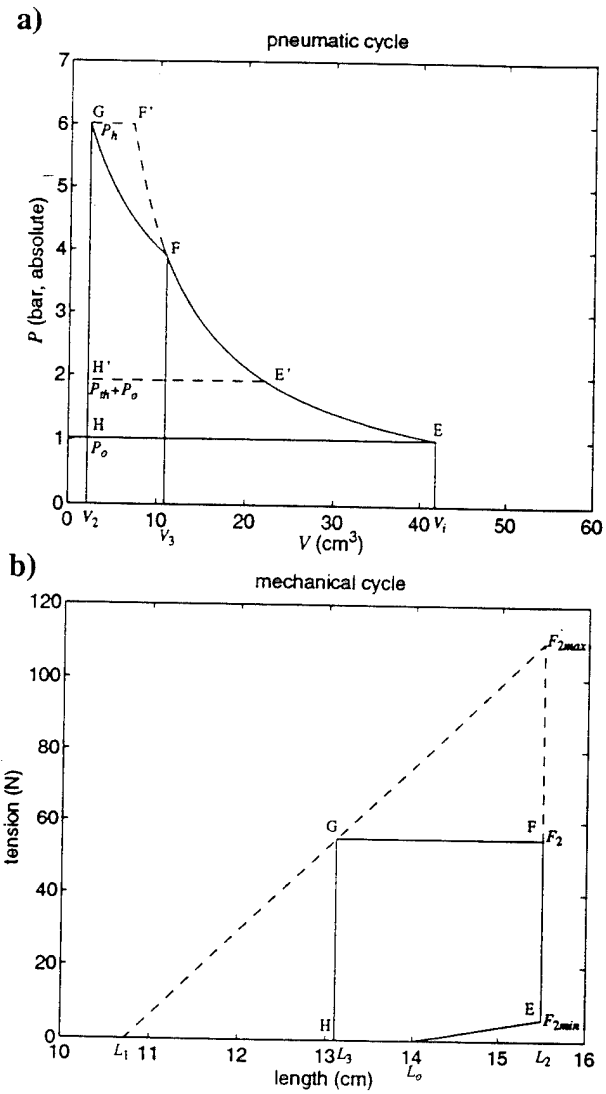
a)
pneumatic cycle
P (bar, absolute)
V (cm3)
G
F'
F
H'
H
E'
E
b)
mechanical cycle
tension (N)
length (cm)
G
F
H
E

Fig.13

properties	units	McKibben actuators @ 5 bar			Biological muscles
		Nylon shell	Fiberglass sheli	Bridgestone	
Resting length (L_o)	cm	14.0	20.0	14.7	
Dynamic range	L_o	0.75 - 1.1	0.85 - 1.15	0.78 - 1.02	0.64 - 1.12
Maximum tension	N	110 @ 1.1 L_o	56 @ 1.15 L_o	260 @ 1.02 L_o	
Stiffness	N/L_o	322	185	1090	
Work per cycle	NL_o	19	8.4	31	
Cross section area	cm^2	0.95 @ 0.75 L_o	0.64 @ 0.85 L_o	1.8 @ 0.78 L_o	
Tension intensity	N/cm^2	116	88	144	35
Stiffness intensity	$N/L_o cm^2$	340	290	606	73
Work density per cycle	J/cm^3	0.20	0.13	0.17	0.13
Coulomb friction	N	2.5	5	5	0
Maximum velocity	L_o/s	> 8			2 - 8 or 20
Average power density	W/cm^3	1.1			
Peak power density	W/cm^3	2.65			0.70
Energy efficiency	-	0.32 - 0.49			0.2 - 0.25

Table 1: The mechanical properties of the McKibben actuators and biological muscles

Submitted to IEEE Intl. Conf on Robotics and Automation, San Diego, May 1994.

Static and Dynamic Characteristics of McKibben Pneumatic Artificial Muscles

Ching-Ping Chou and Blake Hannaford

Department of Electrical Engineering, FT-10, University of Washington, Seattle, Washington 98195

Abstract: This paper reports mechanical testing and modeling results for the McKibben artificial muscle pneumatic actuator. This device first developed in the 1950's, contains an expanding tube surrounded by braided cords. We report static and dynamic length-tension testing results and derive a linearized model of these properties for three different models. The results are briefly compared with human muscle properties to evaluate the suitability of McKibben actuators for human muscle emulation in biologically based robot arms.

Introduction

The McKibben pneumatic artificial muscles were developed in artificial limb research in the 1950s and 1960s (Schulte 1961, Gavrilovic and Maric 1969). They have recently been commercialized by the Bridgestone Rubber Company of Japan for robotic applications, and re-engineered by Prof. Jack Winters for construction of biomechanically realistic skeletal models. McKibben muscles consist of an internal bladder surrounded by a braided mesh shell (with flexible yet non-extensible threads) that is attached at either end to fittings or to some tendon-like structure. When the internal bladder is pressurized, the high pressure gas pushes against its inner surface and against the external shell, and tends to increase its volume. Due to the non-extensibility (or very high longitudinal stiffness) of the threads in the braided mesh shell, the actuator shortens according to its volume increase and/or produces tension if it is coupled to a mechanical load. This physical configuration causes McKibben muscles to have variable-stiffness spring-like characteristics, non-linear passive elasticity, physical flexibility, and very light weight compare to other kinds of artificial actuators (Hannaford and Winters 1990).

The relationships between tension, length, velocity, and activation are the major characteristics of actuators which vary greatly from type to type. Human skeletal muscle also has its own particular characteristics: the convex shape active tension-length relationship (Gordon et al. 1966), the non-linear passive tension-length relationship, the hyperbolic tension-velocity relationship (Hill 1938), and each of above also is a function of activation level (McMahon 1984, Winters 1990, Zahalak 1990). In order to show the similarity (or not) to biological muscles, three types of McKibben muscles, two designed and made by Dr. Winters and one manufactured by Bridgestone, were tested.

In this article, 1) an idealized static physical model of McKibben muscles will be analyzed with a simple theoretical approach, 2) a series of quasi-static and dynamic experiments will be described using a dynamic testing machine, which show a velocity independent tension-length hysteresis, 3) a simplified static model will be described based on both experimental data and theoretical approach, and 4) the quasi-static and dynamic characteristics will be analyzed.

Finally, the actuators will be compared to biological muscles. In general, the McKibben artificial muscle is much more similar to biological muscles than other kinds of artificial actuators.

Static physical model of McKibben muscles

McKibben muscle is an actuator which converts pneumatic (or hydraulic) energy into mechanical form by transferring the pressure applied on the inner surface of its bladder into the shortening tension. In order to find the tension as a function of pressure and actuator length, without considering the detailed geometric structure, a theoretic approach from the view of energy conservation is described as following.

The input work (W_{in}) is done in McKibben muscle when gas pushes the inner surface of the bladder, which is:

$$dW_{in} = \int_{S_i} (P - P_o)\, d\mathbf{l_i} \cdot d\mathbf{s_i}$$

$$= (P - P_o) \int_{S_i} d\mathbf{l_i} \cdot d\mathbf{s_i} = P'\, dV \qquad (1)$$

where P is absolute internal gas pressure, P_o, environment pressure (1 atm), P', relative pressure $(P - P_o)$, S_i, total inner surface, $d\mathbf{s_i}$, area vector, $d\mathbf{l_i}$, inner surface displacement, and dV, volume change. The output work (W_{out}) is done when the actuator shortens associated with the volume changes, which is:

$$dW_{out} = -F dL \qquad (2)$$

where F is axial tension, and dL is axial displacement. From the view of energy conservation, the input work should equal the output work if a system is lossless and without energy storage. Assume the actuator is in this ideal condition. We can then use the "virtual work" argument:

$$dW_{out} = dW_{in}, \qquad (3)$$

thus, from equ. 1 and equ. 2,

$$-F dL = P' dV, \qquad (4a)$$

This research was conducted with the support the Office of Naval Research (Grant no N00014-92-J-1401).

$$F = -P' \frac{dV}{dL}. \tag{4b}$$

To estimate dV/dL, the middle portion of the actuator is modeled as a perfect cylinder (Fig.1), where L is the length of the cylinder, θ, the angle between a braided thread and the cylinder long axis, D, the diameter of the cylinder, n, number of turns of a thread, and b, the thread length. L and D can be expressed as functions of θ with constant parameters n and b,

$$L = b\cos\theta, \tag{5}$$

$$D = \frac{b\sin\theta}{n\pi}. \tag{6}$$

The volume of the cylinder is,

$$V = \frac{1}{4}\pi D^2 L = \frac{b^3}{4\pi n^2}\sin^2\theta\cos\theta. \tag{7}$$

So, from equ. 4b, F can be expressed as a function of P' and θ,

$$F = -P' \frac{dV}{dL} = -P' \frac{dV/d\theta}{dL/d\theta} = \frac{P' b^2 (3\cos^2\theta - 1)}{4\pi n^2}, \tag{8a}$$

which is equivalent to

$$F = \frac{\pi D_o^2 P'}{4}(3\cos^2\theta - 1) \tag{8b}$$

where $D_o = b/n\pi$, is the diameter when θ equals 90°, the form used in Schulte's paper (1961)).

The tension is thus linearly proportional to the pressure, and is a monotonic function of the braid angle. The maximal shortening will be reached when $F = 0$, that is, $\theta = 54.7°$. However, if the thickness (t_k) of the shell and bladder is considered, the relation becomes

$$V = \frac{1}{4}\pi (D - 2t_k)^2 L, \tag{9}$$

by plugging into equ. 4b,

$$F = -P' \frac{dV}{dL} = \frac{\pi D_o^2 P'}{4}(3\cos^2\theta - 1)$$

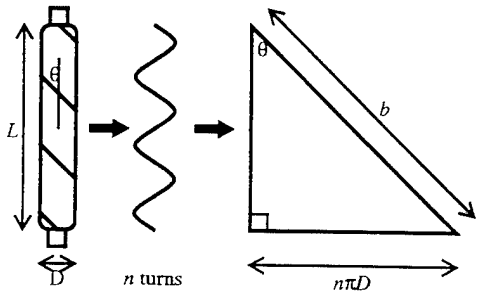

Fig. 1 The geometry of the actuator. The middle portion of the actuator is modeled as a perfect cylinder with length L and diameter D. θ is the angle between a braided thread and the cylinder long axis. n, number of turns of a thread, and b, the thread length. The relationship between the above parameters is illustrated by the triangle.

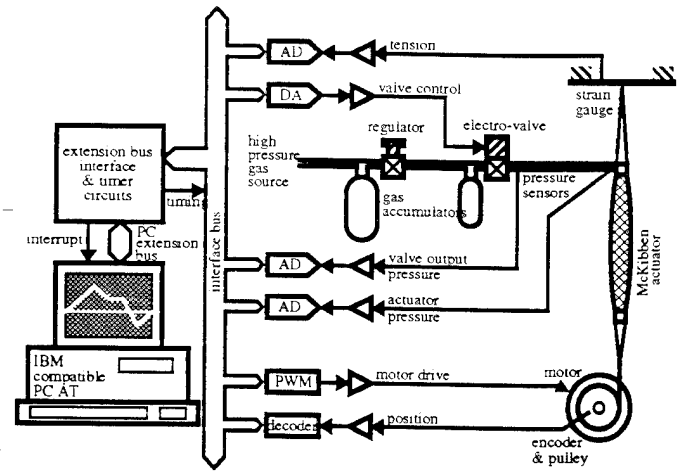

Fig. 2 Block diagram of the dynamic testing machine.

$$+ \pi P' \left[D_o t_k (2\sin\theta - \frac{1}{\sin\theta}) - t_k^2 \right]. \tag{10}$$

This is more complex than equ. 8b.

Quasi-static and dynamic experiments

For the following experiments, a testing system capable of producing and recording desired patterns of the tension, length, and pressure of the actuator was built (Fig.2).

The hardware includes an IBM compatible personal computer (PC), PC extension bus interface and any necessary digital and analog circuits, pressure sensors (6.8 bar max.), a pressure regulator, a electro-valve (10 bar max.), strain gauge force sensors (100 N max.), a 1/4 horse power DC motor, pulse-width-modulation power amplifier (± 24 A max. current), an optical angular position incremental encoder (1600 steps per revolution), and a testing frame (12"w × 20"h × 8"d) to mount the mechanical parts, sensors, and the actuator.The software includes real time position and force control, data acquisition and user interface.

By utilizing different combinations of the I/O channels and software settings, the system can performs a variety of testing conditions, such as constant pressure testing, isometric testing, isotonic testing, pneumatic circuit testing, or fully dynamic testing, etc. However, only the constant pressure testing is applied in this article.

Since there is no analytical solution to describe biological muscle tension-length-activation relationship, a variety of configurations have been choose to illustrate part of this relationship, such as static tension-length relation under constant activation level (Gordon et al. 1966), isometric to isotonic quick release experiment (Gasser and Hill 1924), isokinetic experiment (Gasser and Hill 1924, Levin and Wyman 1927), isometric tension in response to activation (Burke et al. 1976, Chou and Hannaford 1992), etc. Notice that the activation is always as an input to muscle mechan-

ics, and either one of the other two quantities (the tension and the length) may be as an input and the other as an output. The pressure of the actuator is analogous to the activation level and will initially be thought of as an input to the actuator, which will be held as constant as possible in these experiments in order to minimize the effects of the pressure dynamics and thus simplify the analysis.

Three types of actuators were tested in quasi-static experiments and one was also tested in dynamic experiments. The first one with nylon shell is 14 cm resting length, and 1.1 cm in diameter at 5 bar no load. The second one with fiberglass shell is 20 cm in length, 0.9 cm in diameter. And the third one, manufactured by Bridgestone, is 14.7 cm in length, 1.5 cm in diameter

In quasi-static experiments, first, the nylon shell actuator was tested. A set of low frequency triangular wave displacements (relative to resting length, L_o = 14 cm) to best cover the linear tension regions corresponding to different pressure levels are selected as the input. The displacements are set to 1 Hz with large operating range (which yields the peak velocity about 0.5 L_o/s).

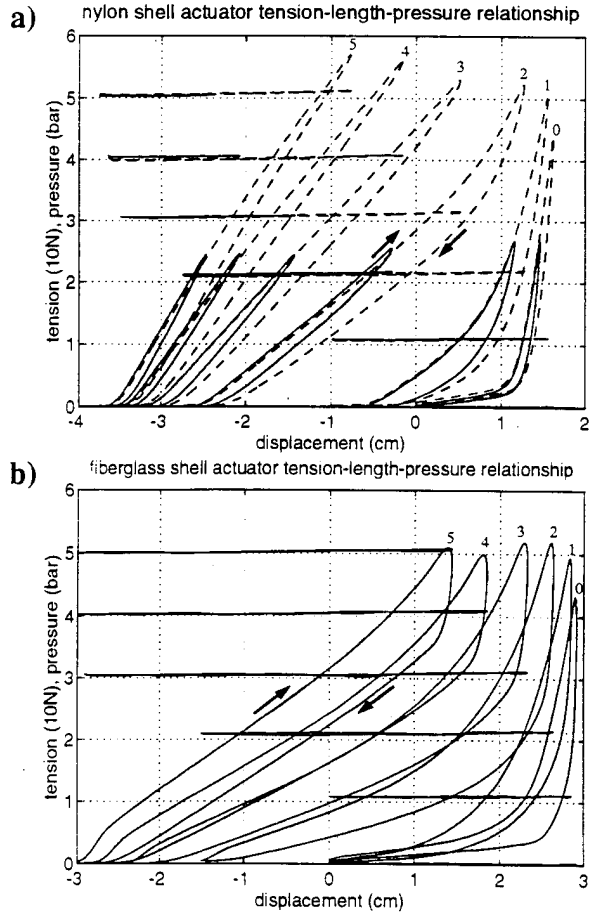

Fig. 3 a and **b** Quasi-static experiments. **a** X-Y plots of the experimental results for the nylon shell actuator. Six pairs of curves are superimposed in the plots: nearly horizontal curves, the measured pressure-length, sloped curves, the tension-length. The hysteresis direction is clockwise. Dashed lines, large range, 1 Hz. Solid lines, small range, 1 Hz. **b** X-Y plot of the experimental results for the fiberglass shell actuator.

The pressure is set by a manual regulator to obtain six desired constant levels (relative 0-5 bar). Due to 1) the volume change of the actuator according to the length change, 2) the gas viscosity in the connection tubing, and 3) the regulator's output hysteresis, the measured pressure will increase when the actuator lengthens and will decrease when it shortens with hysteresis loop. In order to reduce the variation of the pressure, a 10 in^3 (164 cm^3) accumulator is connected to the regulator, and a 3 in^3 (49 cm^3) accumulator is connected directly to the actuator. As a result, the pressure variation was limited to less than 0.1 bar due to the large total capacity of the accumulators, and the pressure hysteresis is almost immeasurable due to the close position (to the actuator) of the second accumulator.

Both the measured pressure and the tension are shown in response to the displacements (Fig.3a, dashed lines). By minimizing the effect of pressure variation, the hysteresis loop of the tension-length relationship is illuminated. The width and height of the loop is about 0.2-0.5 cm and 5-10 N respectively. Two further experiments were made to illustrate more features of the hysteresis.

First, the frequency of the displacement waveforms is reduced to 0.25 Hz, while the operating range remains the same (which yields the peak velocity about 0.125 L_o/s). The result is almost identical to the previous case, which suggests that the tension-length behavior is velocity (low velocity) independent. Second, the frequency is set to 1 Hz, while the operating range is reduced about half (Fig.3a, solid lines). The tension rising paths remain the same (the rising "initial conditions" are the same), but the falling paths are different (The falling "initial conditions" are different due to the smaller operating range). Thus the width and height of the loop are reduced. This indicates the hysteresis is history dependent.

The procedure to obtain Fig.3a was repeated for the fiberglass actuator, and the results in the same format are shown in Fig.3b. Similar tests were performed for the commercially available Bridgestone actuator (Chou and Hannaford 1993). The stiffness, friction, and extensibility are quite different in the above three actuators.

In dynamic experiments, only the first actuator was tested. A set of middle to high frequency sinusoidal displacement waveforms (relative to zero tension length) with small operating range is applied. The pressure is set to relative 5 bar, and remains constant quite well in this condition (due to smaller length change). The frequencies and displacement range are designed to obtain 0.2-8.0 L_o/s peak velocity yet remain in the linear tension-length region. The viscous friction (damping force) if measurable, would be revealed by a hysteresis width which is a mono-

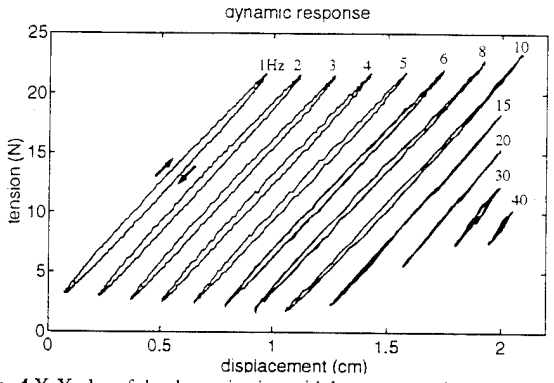

Fig. 4 X-Y plot of the dynamic sinusoidal responses. the results for 12 frequencies are combined together with shifting. Notice the width of the hysteresis is almost unchanged for peak velocity from 0.2 L_o/s (1 Hz) to 2.0 L_o/s (10 Hz). The hysteresis direction is clockwise.

tonic increasing function of the velocity. However, the results show that the width of the tension-displacement loop is very small and almost unchanged, except for a slight decrease at higher frequency (Fig.4).

These results indicate that the velocity-independent hysteresis is most likely to be the Coulomb friction, which dominates the total friction of the actuator. The viscous friction is much smaller than Coulomb friction and thus immeasurable.

An attempt to reduce the Coulomb friction was performed by applying three types of lubricant (including "WD-40 stops squeaks", 10W-40 engine oil, and another kind of small machine oil) on the braided shell and bladder of the nylon actuator. Only 10% of Coulomb friction were reduced by these measures. A special type of lubricant is probably required to reduce the friction of plastic-plastic contacts.

Simplified static model

Excluding the above Coulomb friction, a hypothetical static tension-length relation can be estimated by equ. 10. The actuator can also be considered as a variable-stiffness elastic element, or a "gas spring", where the tension is a function of the pressure and the length. Its stiffness ($K \equiv dF/dL$) is proportional to the pressure, and the stiffness per unit pressure ($K_g \equiv dK/dP'$) approximates a constant within 10 to 14 cm length by simulation (K_g = 0.461 cm, or 4.61 N/cm·bar, with estimating the effective thickness t_k = 0.0762 cm and the diameter D_o = 1.66 cm). So, fortunately, it can be linearized as:

$$F = K_g P' (L - L_{min}) \qquad (11)$$

where L_{min} is the theoretically possible minimum length (when $F = 0$).

Consider energy stored by the actuator in its bladder and shell, yielding

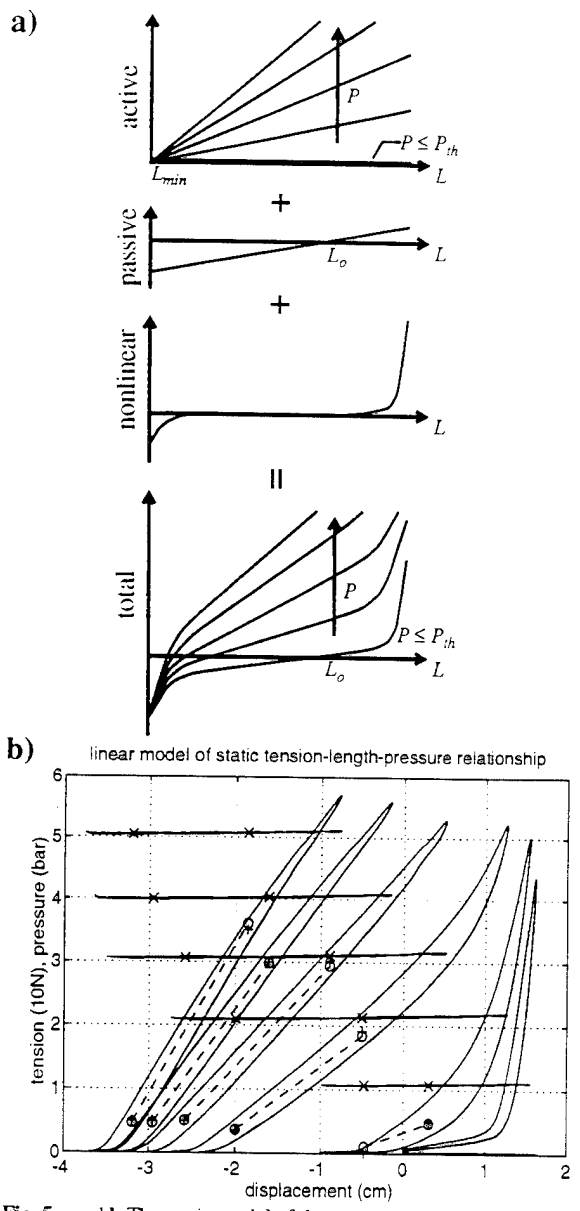

Fig. 5 a and **b** The static model of the actuator. **a** the total tension is the summation of the active term, passive term, and non-linear term. **b** The parameters of the linearized model are optimized with 10 tension-length-pressure sample points from experimental data of Fig. 3a. x, sampled pressure, +, sampled tension, o, simulation tension.

$$F = K_g (P' - P_{th})\ (L - L_{min}) + K_p (L - L_o) + nl(L) \qquad \text{if } P' > P_{th}, \text{ or} \qquad (12a)$$

$$F = K_p (L - L_o) + nl(L) \qquad \text{if } P' \le P_{th} \qquad (12b)$$

where P_{th} is the threshold for the pressure to overcome the radial elasticity of the bladder for expanding, K_p is the linearized equivalent parallel passive elastic constant for the shearing force of the bladder material and shell threads, and $nl(\cdot)$ is the non-linear term due to the non-perfect cylinder while the actuator is at its extreme length (Fig.5a). The first

two product terms in equ. 12a can be expressed as

$$F = K_g (P' - P_a) (L - L_{min}) + F_a \qquad (13)$$

where $P_a = P_{th} - K_p / K_g$, and $F_a = K_p (L_{min} - L_o)$. To experimentally estimate these parameters, 10 points of hypothetical static tension-length-pressure pairs are sampled from above quasi-static results and fit into equ. 13 (Fig.5b), thus obtain K_g = 0.466 cm, P_a = 0.062 bar, L_{min} = 9.91 cm, and F_a = -16.0 N. Also, P_{th} and K_p can be estimated by knowing L_o = 14.0 cm, which yields P_{th} = 0.903 bar and K_p = 3.92 N/cm. Notice the K_g is very close to the theoretical value 0.461 cm. The non-linear term only becomes significant when the actuator is extremely short or extremely long, usually this is out of regular operating range, and will not be discussed further.

Quasi-static and dynamic characteristics

It has been shown that there is hysteresis in the tension-length cycle, and that the dominant friction is the frequency insensitive Coulomb friction, which is caused by the contact between the bladder and the shell, between the braided threads and each other, and the shape changing of the bladder. The history dependence makes the friction difficult to predict precisely, especially after the actuator is attached to artificial bones with curving shape. So, it is suggested to add a typical friction value (± 2.5 N, positive for lengthening, negative for shortening) to the hypothetical static equation (equ. 12a or 13 and 12b) if simplicity is necessary.

Summary

We have measured the mechanical characteristics of the McKibben muscles (the actuators), which behaves like a variable-stiffness elastic element with velocity-insensitive friction. The stiffness is mostly dependent on the internal gas pressure, however, in order to produce tension, the pressure must be higher than a threshold to overcome the radial elasticity of the bladder. Also, a piecewise-linear, static model of the McKibben muscle has been built. The format of the model was simplified and linearized from theoretical results, and the parameters were optimized with experimental data. The friction, although insensitive to velocity, is history dependent, and thus is difficult to model. A constant Coulomb friction was suggested and integrated into the static model to obtain a dynamic model.

Discussion

In the following, comparisons will be given between the McKibben muscles and biological skeletal muscles in terms of static and dynamic properties.

1) Static properties: tension-length-activation relationships

The general shape of the tension-length curve of the actuators is a monotonic increasing function of the length. For the tested nylon shell actuator, the tension reaches zero when the length is shorter than 0.75 L_o (L_o = 14 cm), and becomes very stiff when the length is longer than 1.1 L_o. Between these two points, the stiffness is about constant with a typical value of 23 N/cm (322 N/L_o) at 5 bar, and is approximately proportional to the pressure with some offset. The maximum tension is 110 N at 1.1 L_o and 5 bar. The integration of the tension within 0.75 to 1.1 L_o is 19 NL_o, which is the maximum output work per mechanical cycle.

In order to calculate the stiffness and tension intensities per unit cross section area and the work per unit volume, we use the external cross section area at maximal shortening as the divider, because this is the maximum cross section area which the actuator should be allowed to occupy in a limb segment. For the nylon shell actuator, the cross section area is 0.95 cm^2 at 0.75 L_o, which yields the stiffness intensity of 340 N/$L_o cm^2$, the maximum tension intensity of 116 N/cm^2, and the work per cycle per unit volume of 0.20 J/cm^3.

The above properties of the other two actuators (fiberglass shell and Bridgestone) are listed in Table 1. The way that the threads form the external braided shell of the actuators influences most differences between the three actuators. The nylon shell actuator consists of a low thread density, middle thickness threads, middle resting braid angle shell, which yields the widest 35% dynamic range, highest work density, and smallest Coulomb friction. The fiberglass shell actuator consists of a high thread density, thin threads, large resting braid angle shell, which yields the largest 15% extensibility, lowest tension and stiffness intensities, and lowest work density. The Bridgestone actuator consists of a high thread density, thick threads, small resting braid angle shell, which yields the narrowest 24% dynamic range, almost no extensibility, and the highest tension and stiffness intensities.

For biological muscles, the tension-length relation can be described by the "active tension" with a trapezoidal shape and the "passive tension" with increasing stiffness when stretched beyond a certain length. There may be a local maximum of the total tension if the increase of passive tension is less than the decrease of active tension to the length. The zero-tension lengths of the active tension are 0.64 and 1.8 L_o (frog striated muscle, Gordon et al. 1966), however, if we define the dynamic range of biological muscles by the non-negative-slope region of the active tension-length curve, then it is within 0.64 to 1.12 L_o. The maximum tension intensity is about 35 N/cm^2 (Guyton 1986, or 30 N/cm^2 from Gordon 1989), this yields the average stiffness intensity of 73 N/$L_o cm^2$, and the work per cycle per unit volume of 0.13 J/cm^3 by numerically integrating the tension-length curve within the dynamic range.

In summary, the biological muscle can be stretched beyond its resting length much longer than the actuators,

but usually this is beyond the ordinary physiological operating region. Also, the biological muscle can shorten a little more than the actuators, this is a major disadvantage of the actuators. On the other hand, the tension intensity of the actuators is much higher than biological muscles, this is a major advantage of the actuators and yields higher work density and stiffness intensity. Finally, to improve the match to biological muscle static properties, passive parallel and serial elastic elements, which exist in biological muscles, can be added into the actuators without difficulty.

2) Dynamic properties: tension-velocity relationships

The tension-velocity relation of the nylon shell actuator, if we do not count the viscosity of the pneumatic circuit, is dominated by a velocity-insensitive Coulomb friction, and the velocity-dependent viscous friction is immeasurable (below 8 L_o/s velocity at least), which yields a very high maximum velocity in theory.

On the other hand, the hyperbolic tension-velocity curve of biological muscles indicates the viscosity decreases when the velocity increases (Hill 1938), and there is no Coulomb friction reported. The typical maximum shortening velocity is 2 L_o/s for slow muscle and 8 L_o/s for fast muscle (Winters 1990) or 20 L_o/s for fast muscle (Gordon 1989).

Obviously the tension-velocity relationship of the actuator is not similar to that of biological muscles. Fortunately, the viscous friction is very small and thus we can add some parallel viscous elements to simulate biological muscles. In addition, although the lubricants used in quasi-static experiments do not significantly reduce the Coulomb friction, there may be some other kinds of lubricant which are more effective.

properties	units	McKibben actuators @ 5 bar			Biological muscles
		Nylon shell	Fiberglass shell	Bridge-stone	
Resting length (L_o)	cm	14.0	20.0	14.7	
Dynamic range	L_o	0.75-1.1	0.85-1.15	0.78-1.02	0.64-1.12
Maximum tension	N	110 @ $1.1L_o$	56 @ $1.15L_o$	260 @ $1.02L_o$	
Stiffness	N/L_o	322	185	1090	
Work per cycle	NL_o	19	8.4	31	
Cross section area	cm^2	0.95 @ $0.75L_o$	0.64 @ $0.85L_o$	1.8 @ $0.78L_o$	
Tension intensity	N/cm^2	116	88	144	35
Stiffness intensity	$N/L_o cm^2$	340	290	606	73
Work density per c.	J/cm^3	0.20	0.13	0.17	0.13
Coulomb friction	N	2.5	5	5	0
Maximum velocity	L_o/s	> 8			2-8 or 20
Avg. power density	W/cm^3	1.1			
Peak power density	W/cm^3	2.65			0.70
Energy efficiency	-	0.32-0.49			0.2-0.25

Table 1: The mechanical properties of the McKibben actuators and biological muscles

Conclusion and future work

The linearized mechanical model of the actuator gave us simple yet accurate descriptions of the actuator behaviors. This can be used in simulation of single or multiple actuator systems for designing consideration.

The static mechanical features of the actuator are very similar to biological muscles, except the dynamic range is narrower and the tension intensity is much higher. Some dynamic features may need to be modified to get even closer, for examples: add some parallel and serial elastic elements in order to fine tune the passive elastic characteristics, use lubricant to reduce the Coulomb friction and add some viscous material to increase the viscous friction in order to fit the tension-velocity relationship.

References

Burke R E, Rudomin P and Zajac F E (1976) The effect of activation history on tension production by individual muscle units. Brain Res. 109: 515-529

Chou C-P and Hannaford B (1992) Dual stable point model of muscle activation and deactivation. Biol. Cybern. 66: 511-523

Chou C-P and Hannaford B (1993) Systematic analyses of McKibben pneumatic artificial muscles. Submitted to IEEE Trans. Robotics and Automation

Gasser H S and Hill A V (1924) The dynamics of muscular contraction. Proc. R. Soc. B 96: 398-437

Gavrilovic M M and Maric M R (1969) Positional servo-mechanism activated by artificial muscles. Med. & Biol. Engng. 7: 77-82

Gordon A M, Huxley A F and Julian F J (1966) The variation in isometric tension with sarcomere length in vertebrate muscle fibers. J. Physiol. 184: 170-192

Gordon A M (1989) Contraction in skeletal muscle. In: Textbook of physiology, vol 1: excitable cells and neurophysiology, chap 8, 21st edn. Seattle, Washington

Guyton A C (1986) Contraction of skeletal muscle. In: Textbook of medical physiology, chap 11, 7th edn

Hannaford B and Winters J M (1990) Actuator properties and movement control: biological and technological models. In: Multiple muscle systems, Winters J, Woo S (eds). Springer-Verlag, New York

Hill A V (1922) The maximum work and mechanical efficiency of human muscles and their most economical speed. J. Physiol. 56: 19-41

Hill A V (1938) The heat of shortening and the dynamic constants of muscle. Proc. R. Soc. B 126: 136-95

Levin A and Wyman J (1927) The viscous elastic properties of muscle. Proc. R. Soc. B 101: 218-243

McMahon T A (1984) Fundamental muscle mechanics. In: Muscle, reflexes, and locomotion, chap 1, Princeton University Press, Princeton, New Jersey

Schulte H F Jr (1961) The characteristics of the McKibben artificial muscle. In: The Application of external power in prosthetics and orthotics. National Academy of Sciences-National Research Council, Washington D. C.

Winters J M (1990) Hill-based muscle models: a system engineering perspective. In: Multiple muscle systems, Winters J, Woo S (eds). Springer-Verlag, New York

Zahalak G I (1990) Modeling muscle mechanics (and energetics) In: Multiple muscle systems, Winters J, Woo S (eds). Springer-Verlag, New York